The Pennsylvania State University

The Graduate School

College of Engineering

CHARACTERIZATION OF POLYMERIZATION-INDUCED WORKPIECE DISTORTION IN PHOTO-ACTIVATED ADHESIVE WORKHOLDING

A Thesis in

Industrial Engineering

by

Kristopher Robert Doll

Submitted in Partial Fulfillment
of the Requirements
for the Degree of

Master of Science

August 2014

The thesis of Kristopher Robert Doll was reviewed and approved* by the following:

Edward C. De Meter
Professor of Industrial Engineering
Thesis Adviser

Christopher Saldana
Assistant Professor of Industrial Engineering

Paul M. Griffin
Professor of Industrial Engineering
Head of the Department of Industrial Engineering

*Signatures are on file in the Graduate School.

Abstract

Photo-Activated Adhesive Workholding (PAAW) is a new technology that offers fixturing solutions for hard-to-hold manufactured components through the use of temporary UV-cured adhesive joints. One area in need of further development is the handling of compliant workpieces. Adhesive joints experience a decrease in volume as they cure, causing either an accumulation of residual stresses inside the adhesive joint or a distortion of the bonding substrates. Compliant workpieces will elastically distort as these PAAW joints polymerize, making it difficult to achieve tight tolerances as these workpieces are processed.

This work characterizes the distortion caused by PAAW adhesive joints in response to factors such as workpiece compliance, joint thickness, and adhesive joint diameter. Empirical models are fit to the experimental data to predict workpiece distortion.

The bonding surfaces, known as Grippers, used in PAAW technology transmit a non-uniform distribution of curing light intensity to the adhesive joint by design. The interaction of adjacent adhesive regions with different light intensities and consequently different polymerization rates is explained in terms of a support column model, where the region that develops a significant elastic modulus first will oppose further motion of the substrate. This idea is demonstrated through experiments with varying adhesive joint diameter.

To offer insight regarding workpiece distortion reduction for typical industrial use of PAAW fixturing, a scenario involving multiple adhesive joints curing simultaneously and sequentially is explored. A methodology is created to predict the resulting distortion of a workpiece for any PAAW fixturing setup and curing sequence. A case study with experimental results validates the approach.

In an attempt to find a low distortion adhesive, a number of different types of filler content and adhesive base resin are evaluated. The adhesive strength, cohesive strength, tensile properties, polymerization shrinkage, and the resulting workpiece distortion are experimentally determined. A model is presented to explain how several of these factors contribute to distortion.

Contents

List of Figures

List of Tables

Acknowledgments

I would like to thank my advisor, professor Edward De Meter for his guidance, dedication, and patience as I completed my thesis. I would also like to thank Dr. Christopher Saldana for reading and providing excellent feedback on my thesis. Special thanks to Dan Supko and Travis Richner for assisting me with the fabrication of the research equipment used in this thesis. I would also like to thank Dr. Wells Cunningham of CTECH for formulating the adhesives used in this work and providing data on those adhesives.

Chapter 1

INTRODUCTION

1.1 Background

Photo-activated Adhesive Workholding (PAAW) is an emerging technology developed at the Pennsylvania State University by Professor Edward De Meter for fixturing hard-to-hold workpieces. A truly flexible workholding technology, PAAW provides solutions for holding workpieces made of virtually any material, having any surface finish, with considerable geometric error, and with any amount of geometric complexity.

A PAAW system works by bonding the workpiece to a fixture using a discrete number of UV-curable adhesive joints. These joints hold the workpiece firmly in place as it undergoes manufacturing operations. At the conclusion of these operations, the adhesive joints are broken and cleaned from the part and fixture.

1.2 Problem Statement

Currently, polymerization induced workpiece distortion presents a major barrier to the adoption of PAAW technology for compliant workpieces. When the adhesive cures, it experiences a certain amount of volumetric shrinkage resulting from the formation of polymer chains. When the workpiece has great stiffness, adhesive in the joint is drawn radially inwards and the remaining axial shrinkage translates into residual tensile stresses rather than workpiece distortion. For workpieces with low stiffness, the workpiece will be drawn

towards the shrinking adhesive joint, resulting in more distortion

The understanding of this behavior is limited and there are no methods for predicting or experimentally measuring the distortion in a workpiece as a function of workpiece stiffness, joint thickness, and other variables. Furthermore, understanding how the composition of an adhesive affects its tendency to distort parts would be valuable for formulating low-distortion adhesives.

1.3 Thesis Goals and Objectives

This work will address many of the issues related to polymerization induced workpiece distortion. Specifically, it will do the following:

1. Present a test apparatus capable to measuring workpiece distortion as a function of workpiece stiffness and adhesive joint size and thickness

2. Create an empirical model to describe the workpiece distortion as a function of the aforementioned variables

3. Investigate the effects of non-uniform curing light distribution found in PAAW adhesive joints on its polymerization behavior

4. Explore the response of a workpiece to multiple adhesive joints curing simultaneously or sequentially and compare this to single joint behavior

5. Expand the single joint model to predict the distortion in a workpiece from multiple adhesive joints

6. Characterize the effects of adhesive base resins and filler content on the mechanical properties of the adhesive and its tendency to distort workpieces

The underlying goal is to provide the reader with an understanding of the factors that affect workpiece distortion or residual stress accumulation in an adhesive joint, methods to

predict the distortion in a system with adhesive joints, and strategies to reduce workpiece distortion.

1.4 Research Scope

The models and results found in this work apply directly to adhesive joints whose adhesive composition, joint geometry, and curing light intensity and distribution is characteristic of the PAAW process.

1.5 Impact on Engineering Practice

The findings presented in this work will offer insight into developing photo-curable adhesives for applications that demand minimal substrate distortion. It will provide a means for estimating the anticipated workpiece distortion in a PAAW fixturing system which process engineers may use to guide them in the design of a PAAW fixture.

The results of this work are not limited to the domain of PAAW technology. Industries that assemble products with photo-cured adhesives, such as optics and electronics packaging, may benefit from the techniques for predicting workpiece distortion.

1.6 Impact on Engineering Science

The concepts explored and the models created will enhance the scientific community's understanding of effects of substrate stiffness, adhesive joint geometry, and adhesive filler content on polymerization induced substrate distortion.

1.7 Thesis Overview

Chapter 2 gives a background on PAAW technology and key principles of adhesive joints. Chapter 3 reviews the literature on shrinkage related distortion and stress accumulation

in adhesives. Chapter 4 provides a summary of the research methodology. A description of the distortion test apparatus developed for this work is given in chapter 5. Chapters 6 through 9 discuss the individual experiments and results. A summary of the key findings and a list of areas for future investigation are given in chapter 10.

Chapter 2

BACKGROUND

2.1 PAAW Technology

Photo-Activated Adhesive Workholding (PAAW) technology was developed by Professor De Meter at the Pennsylvania State University as a fixturing solution for hard-to-hold parts [1]. PAAW systems can be used for workpiece holding in industrial machine tools and in coordinate metrology machines. Blue Photon Technology and Workholding Systems LLC develops and manufactures the equipment for PAAW systems.

The technology consists of several basic components:

Grippers The grippers serve as the adhesive bonding substrate that are fastened into the workholding fixture. They consist of a hardened steel chassis surrounding a transparent sapphire window to transmit UV light to the adhesive joint (figure 2.1). Grippers produced by Blue Photon come in two general sizes, 250 and 330. The 250 grippers feature a .250 inch (6.35 mm) diameter sapphire window and the 330 grippers have a .330 inch (8.38 mm) window. The chassis diameters of the 250 and 330 grippers are 12.4 and 15.5 mm, respectively.

Adhesive Developed specifically for PAAW, GB1 is a UV curable acrylate-based structural glass-bonding adhesive that features high adhesive and cohesive strength (figure 2.2). It contains fumed silica to give it a gel consistency so that it may stay on grippers at vary-

Figure 2.1: 250 and 330 head-out style PAAW grippers

Figure 2.2: GB1 PAAW adhesive

ing orientations prior to curing. It has rubber impact modifiers to give it the toughness necessary to survive under heavy milling conditions. Furthermore, a generous package of photo-initiators allows adhesive directly above the gripper chassis to cure quickly in spite of the reduced light power reaching that region.

High intensity UV curing lamp A spot lamp provides the ultra-violet radiation necessary to activate the photo-initiators and polymerize the adhesive. With a system such as the Dymax BlueWave 200 (figure 2.3), a typical PAAW adhesive joint can be cured to sufficient work-holding strength with a 30 to 60 second exposure. For added consistency, spot lamps may have features for controlling exposure duration and UV light intensity. Light intensity in the UVA spectrum can be measured with a radiometer (figure 2.4)

Light guides These channel the UV radiation from the spot lamp to the grippers. The light guide core may contain either a bundle of optical fiber or a liquid. Light guides give the PAAW system great flexibility with regard to the placement of grippers in a fixture. To allow for increased productivity, light guides may divide the source light across multiple ends. Figure 2.5 shows a variety of light guides: an 8mm, a 5mm, and a 3mm which

Figure 2.3: High intensity UV spot lamp

Figure 2.4: UVA radiometer

distributes light four ways.

In a properly designed PAAW fixture, the workpiece will rest against locating features above a series of grippers that are fastened to the fixture. Prior to the installation of the workpiece, a small amount of adhesive is applied to each gripper. The workpiece is then placed on the fixture, and a light guide connecting to a UV lamp is inserted behind a gripper through the backside of the fixture. The shutter of the lamp opens for a set duration and the adhesive between the gripper and the workpiece photo-polymerizes to create a strong joint. This process is repeated for all the grippers in the fixture. The end result is a workpiece that is rigidly bonded to the fixture.

The workpiece then undergoes a sequence of manufacturing operations while bonded to the fixture. To remove the part when finished, the adhesive joints are destroyed by rotating the grippers within the fixture. This creates a condition of pure shear in the adhesive joint

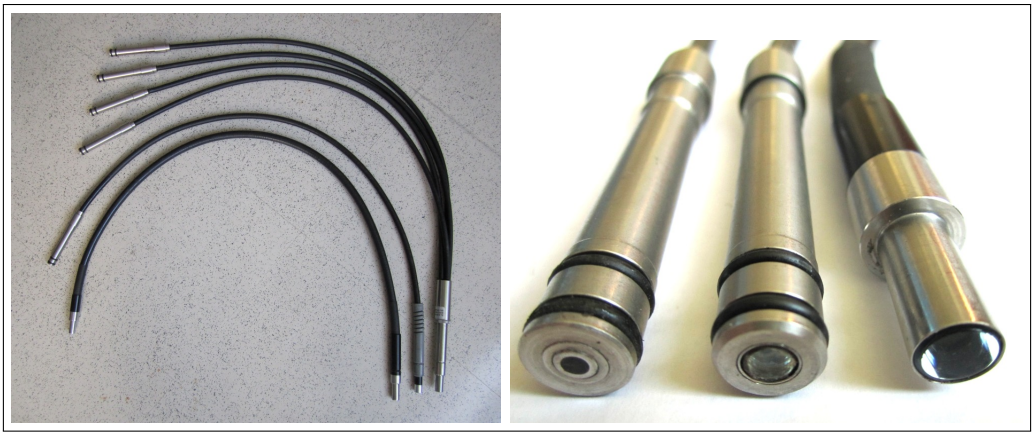

Figure 2.5: Light guides

that will break the joint while minimizing the stress transmitted to the workpiece.

Cured adhesive from the broken joints will remain on the surface of the grippers and the workpiece. The residual adhesive on the grippers can be removed quickly and efficiently with specially designed spindle-mounted grinding tools. The remnants of the adhesive joint on the workpiece are typically removed using a high-pressure hot water spray. Alternatively, it can be removed during subsequent machining operations or manually.

The advantages of a PAAW system compared to conventional mechanical clamping fixtures include the following:

- Ability to hold workpieces that lack convenient clamping locations.
- Increased rigidity from being able to hold the undersides of parts. This helps dampen mechanical vibration.
- Great tolerance for geometric variability of workpiece. PAAW joints may range in thickness from .2 to 3 mm.
- 5-sided machining access when grippers are located under the part.
- Simple fixture design. Typical fixtures consist of a plate with a combination of hard contact locators and grippers.

- Setup time reduction for complex parts.

2.2 Photo-polymerization of Acrylate Adhesives

Photo-curable acrylate-based adhesives, such as GB1, contain a number of different components:

- Acrylate monomers
- Photo-initiators
- Filler content and modifiers

When a photo-initiator is exposed to light in its absorption band, one of its electrons is briefly promoted to a higher energy orbital. Quickly thereafter, the electron either decays back to its original state, releasing light and heat, or it forms a reactive intermediate. The reactive intermediate may either react with another free radical or it may react with a monomer to facilitate the formation of polymer chains [2]. The polymerization initiation rate is a function of the intensity of light in the photo-initiator's absorption band, the concentration of photo-initiator, and the fraction of photo-initiator electron excitation events that result in polymerization initiation.

After initiation, the free-radical active center on the monomer continues to react with monomers and propagates the chain. As each new monomer is added to the chain, the active center moves to the end of the chain. This process ends when the radical reacts with a radical on another chain and terminates the chains by either combining both chains to make a longer chain or by forming terminal double bonds on the active centers of both chains [3]. When light exposure stops, free radicals cease being produced, and existing radicals are consumed in termination reactions, ending the polymerization [4]. It has been found that when PAAW adhesive joints are exposed to a critical light intensity, the joint polymerizes at its maximum rate; increasing the intensity further does not reduce the curing time [5].

As an adhesive begins curing, the accumulation of polymer chains increases its viscosity. At a certain critical degree of conversion, known as the gel point, the viscosity approaches infinity. After this point, the adhesive acts like a solid and starts developing an elastic modulus. Stress relaxation occurs most readily prior to or immediately following the gel point [3].

Polymerization shrinkage is caused by the creation of covalent bonds between monomers that were previously held together by van der Waals forces, which reduces their separation distance by a factor of 2 [3]. When unrestrained, volumetric contraction, β, of the adhesive is related to the linear shrinkage, α in the following equation:

$$\beta \approx 3\alpha \tag{2.1}$$

Inert fillers, such as SiO_2 spheres and hollow micro-balloons, are typically added to adhesives to reduce volumetric shrinkage and improve mechanical properties. Fumed silica can be added to increase the adhesive's viscosity.

Chapter 3

LITERATURE REVIEW

3.1 Application of Adhesive Fixture Systems

This work revolves around the PAAW fixturing system developed at the Pennsylvania State University by De Meter [1]. De Meter and Kumar thoroughly investigated the factors that affect the lead time, machining cost, and part quality of a PAAW system and present a methodology for analyzing the economic viability of such a system [6].

Adhesive workholding systems are capable of handling aggressive machining conditions of common aerospace superalloys in typical industrial setups [7]. Other types of adhesive systems can bond flexible electronic workpieces to rigid substrates for chemical and thermal processing operations [8].

Raffles et al. have suggested alternative methods for debonding delicate workpieces such as pin-array systems that shield the workpiece from the debonding forces or the use of resistive or inductive heating elements to thermally destroy adhesive joints [7]. In the realm of flexible electronics workholding, subjecting the adhesive to additional UV radiation will cause it to lose its ductility and to experience increased polymerization and thermally induced strains. When it exceeds its maximum strain, it peels away from the workpiece and tooling surfaces [8].

Cai et al. review methods of determining the optimal fixture design for compliant workpieces [9].

3.2 Methods for Characterizing Adhesive Shrinkage and Related Properties during Polymerization

The main factor in workpiece distortion or residual stress accumulation is the amount of shrinkage that the adhesive undergoes during curing. Polymerization shrinkage of an adhesive is traditionally measured in a water or mercury dilatometer. However, this method is not as suitable for photo-cured polymers because of difficulty exposing the adhesive to light without it being attenuated by the liquid and the issue of the curing light raising the temperature of the fluid and thermally expanding it [10].

Watts and Cash developed what is known as the Bonded Disc Method for measuring polymerization shrinkage of photo-curable adhesives [10]. The method consists of curing a small disc of adhesive between a transparent plate and a very compliant substrate, such as a microscope slide. Light is applied through the plate, and a displacement gauge measures the resulting deflection of the compliant substrate. When the adhesive disc has an diameter to thickness ratio exceeding 9, the volumetric shrinkage of the adhesive can be very closely approximated by the shrinkage in the axial direction [11]. If the adhesion between the adhesive and substrate is poor, this method will instead obtain the linear shrinkage of an unbonded adhesive [12].

Lee et al. created an instrument that can determine volumetric shrinkage by measuring changes in the bouyancy force of an adhesive submerged in water [12]. Hudson et al. measured the polymerization shrinkage of an adhesive drop by taking digital images of the drop before and after polymerization determining the change in its volume [13].

Elastic modulus can be measured in number of different methods: The stress-strain response of an adhesive at several points during polymerization can be measured by introducing strain pulses in the joint while measuring force [14]. Shear modulus can be found using a rheometer that applies an oscillating shear strain to a polymerizing joint and measures the resulting shear force [15]. Elastic modulus of a cured specimen can be determined

from its resonant frequency detected with a microphone [16] [17].

There are several methods for measuring the developing stress or strain due to polymerization shrinkage on a system: Kleverlaan and Feilzer used a tensilometer with position feedback control to measure the contraction stresses of adhesive joints during polymerization under constant joint thickness [18]. Lee et al. designed a Stress-Strain Analyzer that features a cantilever beam and a servo-driven crosshead with feedback control that can measure adhesive joint stress and strain during polymerization for two levels of system compliance [19]. With this device and measurements from a bonded disc method apparatus and a rheometer, these researchers could draw correlations between stress accumulation, elastic modulus development, and volumetric shrinkage during polymerization [15].

3.3 Modeling Approaches

There are several researchers using finite element analysis to predict the residual stress state in an adhesive joint or the related substrate distortion. A popular method of simulating the polymerization shrinkage consists of setting the thermal expansion coefficient equal to the volumetric shrinkage factor and displacing the temperature by one unit. Laughlin et al. used this technique to map the residual stress state in adhesive joints for a number of different substrate stiffnesses [20].

Analytical models for predicting joint stress and strain also exist. Petrovic et al. formulated a closed form solution based on classical diffusion models with the assumption that shrinkage strain rate is proportional to reaction rate [21]. Dauvillier et al. present a model that captures the visco-elastic behavior of an adhesive during polymerization [14]. Patankar et al. created analytical models to predict thermally induced distortion, stresses, and visco-elastic stress relaxation of adhesive joints bonded to compliant workpieces [22].

In addition to capturing the effects of polymerization shrinkage, it is also important in the PAAW application to be able to model a system with adhesive joints. Castagnetti and Dragoni provide an overview of finite element modeling approaches and simplifications for

analyzing parts with adhesive joints [23]. De Meter has explored finite element modeling of PAAW joints and validated modeling assumptions with experiments measuring the effective tensile and shear strengths of PAAW joints [24]. Lee and Haynes discuss how to model frictional behavior of traditional fixturing clamps in a Finite Element model [25].

Also related is the light intensity reaching the adhesive joint, as this dictates the reaction rate and may influence the joint's degree of conversion. Baker and De Meter have experimentally measured and modeled the light transmission through an adhesive joint during polymerization [26].

3.4 Methods for Reducing Adhesive Polymerization Distortion or Stress Accumulation

There are four main concepts to reduce the accumulation of distortion or stress during polymerization:

1. Minimize the overall volumetric shrinkage of the adhesive using inert filler material
2. Adjust the process to allow the adhesive to relieve stresses prior to the development of a substantial elastic modulus
3. Cure the adhesive in increments so to take advantage of a small ratio of bonded to unbonded surface area
4. Select a base resin with minimal polymerization shrinkage

The effectiveness of the first strategy is intuitive and well established in practice. Adding inorganic material that does not shrink to an adhesive should theoretically decrease the overall shrinkage by the percent volume of filler. However, rigid filler material will increase the overall elastic modulus of the composite and reduce the ability of the material to flow during polymerization. Spherical filler shapes tend to have a greater effect at reducing volumetric shrinkage than irregular shapes [27]. The influence of filler material size is a more

complicated matter that may be related to the scattering of light and resulting degree of conversion. Interestingly, glass microspheres typically increase the optical transmission of a composite [28]. Glass fibers restrict the strain of the adhesive along the axis of the fibers which may provide additional volumetric shrinkage reduction [29]. Adding to the adhesive gas porosity or filler materials with low elastic moduli may reduce the net volumetric shrinkage at the price of joint strength and stiffness [30].

The second strategy consists of maximizing viscous flow or plastic deformation in the polymer while it is still liquid or has just passed the gel point. Although it seems intuitive, it is unclear that low viscosity adhesives with a low elastic modulus in the cured state result in less stress or distortion [17]. These adhesives tend to have greater volumetric shrinkage that counteracts the benefit derived from a low modulus and greater flowability.

An interesting idea is known as soft start curing [31]. In this process, the adhesive joint is initially briefly exposed to a reduced level of light intensity. The light is removed for some time and then the adhesive is exposed to a full dose of typical curing light intensity. This initial step causes a slow reaction rate that gives the adhesive time to flow and/or stress relieve as it approaches the gel point. The second step ensures that the adhesive reaches an adequate degree of conversion.

In the third strategy, incremental curing of an adhesive joint takes advantage of the small ratio of bonded to unbonded surface areas of each increment to facilitate flow [30]. By allowing viscous or plastic flow away from unbonded surfaces, the shrinkage strain between bonded surfaces may be reduced, resulting in less substrate distortion or residual stress in the adhesive joint. However, the effect of incremental curing on net residual stress can be complicated by rigid body motion of unbonded substrate surfaces [32].

The fourth strategy involves selecting adhesive base resins that use large monomers. Adhesives with monomers of large molar volumes shrink less because volume lost during the formation of covalent bonds is smaller compared to the original volume of the monomer [28].

3.5 Assessment of the Current State of Knowledge

Considering the novelty of the PAAW application, it is no surprise that several elements important to adhesive workholding have not yet been explored in the literature:

- Models, empirical or first principle, that capture the flow of adhesive away from non-bonded surfaces of adhesive joints during photo-polymerization prior to reaching the gel point
- Models that predict the distortion of a workpiece as a function of its stiffness and the adhesive joint thickness
- A method or device for measuring the distortion caused by an adhesive joint for any arbitrary level of workpiece stiffness
- An investigation of the effect of having regions in an adhesive joint exposed to very different curing light intensity on net workpiece distortion
- A methodology for predicting the total workpiece distortion for a series of adhesive joints cured in an arbitrary sequence

It is the aim of this thesis to address these limitations.

Chapter 4

METHODOLOGY

One of the primary interests is how the distortion of a workpiece or residual stress accumulation of the adhesive joint is related to the workpiece stiffness and the joint thickness. In chapter 6, these two variables are explored using the distortion test apparatus described in chapter 5. For each test, an adhesive joint is photo-polymerized between a PAAW gripper and an anvil suspended from a beam. UV light enters the joint through the window in the gripper and a light guide connected to a spot lamp. During the polymerization, the displacement of the anvil and the force transmitted through the beam are recorded, providing a clear picture of the workpiece distortion and the buildup of residual stress. Workpiece stiffness is varied through the use of beams of stiffness ranging from .013 to 114 N/μm. The thickness of the adhesive joint is varied by adjusting the gap between gripper and anvil. Thicknesses ranging from .1 to 2.0 mm are tested. The resulting anvil displacement, or workpiece distortion, for all test levels is used to create an empirical model of the behavior of the adhesive, in this case GB1, fitted to the data with regression analysis.

When photo-curing adhesive joints, there will always be a non-uniform distribution of light through the joint resulting in differences in polymerization rate. This is especially true of PAAW grippers, whose design creates two distinct regions that receive very different levels of light intensity. Specifically, the region directly above the window will be directly exposed to the light exiting the light guide whereas the region above the chassis will receive only the light that scatters outwards. In chapter 7, distortion tests are performed where

the size of the gripper window and the diameter of the adhesive joint are varied to explore how the size of the primary and secondary regions of the adhesive affect the resulting workpiece distortion. Gripper window size is controlled through the use of either 250 or 330 grippers and the joint thickness is a constant 1.5 mm for all tests. Adhesive joint diameter is determined after the test using digital calipers. In another test, a full size joint is exposed for 1 second to the curing light so that the primary region may have just enough exposure to begin polymerizing but the secondary region will be largely unpolymerized. Then the joint is fully cured with a standard duration exposure to the UV light. This process, generally referred to in the literature as soft start curing, will shed light on the combined effect of light distribution and polymerization rate on workpiece distortion.

Of great practical important is understanding the effect of curing multiple joints to a single workpiece either incrementally or at the same time. Equally important is the ability to predict the cumulative effect of the multiple joints on workpiece distortion and how to determine the optimal curing sequence for a particular system. In chapter 8, tests involving two PAAW grippers bonding to a cantilever beam are performed to investigate how the resulting workpiece distortion is affected by the curing strategy (sequential or simultaneous) and how it compares to the distortion from polymerizing individual joints alone. Two levels of workpiece stiffness and three levels of joint thickness (ranging from .4 to 1.4 mm) are included in the evaluation. The resulting distortion of a sequential cure can be predicted by considering the distortion introduced by each joint individually. For each step in the curing sequence, the new joint will distort the workpiece in a manner described by the empirical model found in chapter 6 and change the stiffness matrix of the system. The stiffness matrix after each step can be found for any arbitrary workpiece through finite element analysis. The key to this approach is using appropriate loading conditions for new joints and models or boundary conditions to approximate the behavior of previously cured joints. Several of these approaches are simulated on a model of the distortion apparatus created in the ABAQUS FEA package and compared with the experimentally measured

workpiece stiffness. Overall distortion is computed as a linear sum of the distortion to the workpiece at each step in the curing process.

The mechanical properties of the adhesive will likely have an effect on the extent of distortion it causes in workpieces. The base resin, filler content, and quantity of viscosity and impact modifiers will influence the adhesive's bulk mechanical and optical properties. Chapter 9 investigates these effects with a set of experiments performed on a number of adhesives. These experiments include the following:

- Axial load tests where a joint is destroyed in tension to determine the effective strength
- Tensile tests of modified ASTM D638-10 type-V specimens extended at a strain rate of 12.7 mm/min
- Distortion tests with joint thicknesses of .5 and 1.5 mm and stiffnesses of .64 and 56 N/μm
- Volumetric shrinkage estimation using a .013 N/μm beam with a 330 gripper to create conditions favorable for pure axial shrinkage of the joints much like the Bonded Disc Method of Watts and Cash

Axial load tests and distortion tests were performed on a collection of adhesive base resins. The most promising adhesives were modified with fumed silica and a greater concentration of photo-initiators. Filled variants of these adhesives were created by adding glass microspheres and microballoons and ground pre-polymerized adhesive. These were subjected to the full set of characterization experiments described above. A simple analytical model was created to explain many of the differences in workpiece distortion for the set of adhesives.

Chapter 5

WORKPIECE DISTORTION TEST APPARATUS

5.1 Principal Features of Apparatus

The experimental test apparatus developed for this work is capable of assessing the distortion experienced by a workpiece from a PAAW system. Force transducers record the force developing inside the adhesive joint while a capacitance gauge measures the displacement of the workpiece. The workpiece compliance is controlled through a set of beams of different thickness and material. A series of specially designed nuts control the thickness of the adhesive joint. The modular nature of the system allows PAAW grippers and bonding surfaces of various sizes to be evaluated. In addition, the system can be adapted to determine the effects of curing multiple grippers to one workpiece. The next section will describe the components of the apparatus.

5.2 Design and Functionality of Apparatus

Figure 5.1 shows the apparatus set up to perform a single-gripper distortion test. A gripper, installed in a gripper block, bonds to an anvil, which is supported on a beam held in place by two support columns. A light guide fits through the bottom of the base plate to transmit UV curing radiation through the gripper. A C1 Lion Precision capacitance gage mounted in an adjustable magnetic stand measures the linear displacement of the anvil.

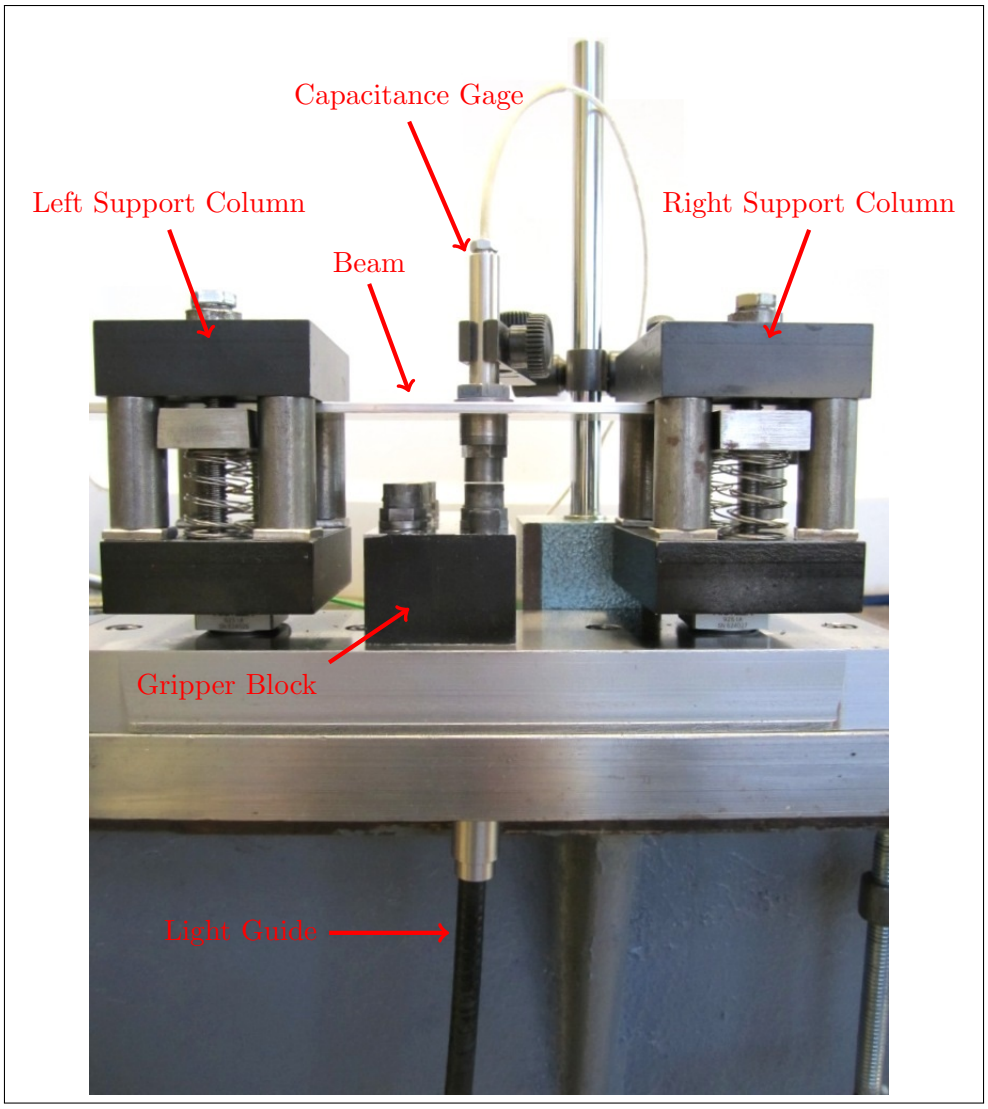

Figure 5.1: Distortion test apparatus

Figure 5.2 shows a close up view of the gap between gripper and anvil which would contain the adhesive joint. When performing a test, a drop of adhesive is placed on either the anvil or gripper surface. The anvil is lowered through the hole in the beam and the weight of the anvil will cause the adhesive drop to fill the joint gap. Excess adhesive flows out the side where it is left undisturbed. Preliminary experiments have demonstrated that the presence of excess adhesive around the gripper does not significantly affect the experimental results.

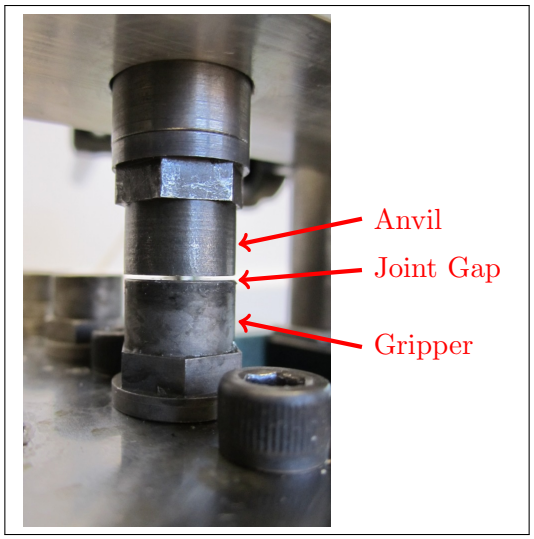

Figure 5.2: Close up view of joint gap

The anvil (figure 5.3) is an interchangeable bonding substrate that is suspended by the beam. The use of these anvils offers several benefits over directly bonding adhesive to the test beams:

- The bonding surface shape and size matches that of the gripper, making the resulting workpiece distortion insensitive to the amount of excess adhesive.
- Anvils covered in cured adhesive following a test can be quickly and easily replaced to perform the next test.
- There is no possibility of damaging the beam from repeated adhesive removal.
- The beam is thermally isolated from the heat generated by the UV radiation. Thermal expansion of the beam is not a factor in anvil displacement.
- The beam is isolated from the radial contraction stresses of the polymerizing adhesive. These stresses have no significant effect on thick beams but can entirely alter the response of very thin beams.

The anvils resembles the 250 series head-out style grippers but do not have a sapphire window. The 12.5 mm outer diameter of the bonding surface matches the diameter of the

Figure 5.3: 12.5 and 15.5 mm anvils

Figure 5.4: Anvils assembled in nuts of varying height

gripper chassis. The anvils are made from 4140 alloy steel hardened to 58-60 HRC for wear resistance. The bonding surface of each anvil was surface ground to facilitate adhesive removal and cleaning. The variation in length of the anvils from their mating surface at the flange to the bonding surface is less than .01 mm. A set of anvils with a 15.5 mm bonding surface diameter were created to use with the 330 series grippers.

Anvils are fastened into anvil nuts which have a flange that seats against the test beam. The anvil nuts allow the experimenter to control the thickness of the adhesive joints. The nuts are identified by the nominal resulting joint thickness they create. Figure 5.4 shows anvil nuts for 2.0, 1.5, .97, and .43 mm joints. Joint gap thickness for each nut was measured using shim gages with a resolution of .025 mm.

A gripper block holds eight grippers as shown in figure 5.5. The block is precision ground to ensure that the bonding surface of all grippers are within .01 mm of the nominal height from the base plate to minimize variability in adhesive joint thickness. The block mounts to the base with the help of two dowel pins for repeatable placement. Under the grippers in the block are holes to receive light guides. The modular nature of the gripper block allows

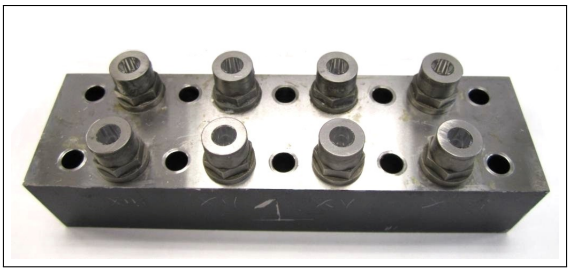

Figure 5.5: Gripper Block with 250 head-out style grippers

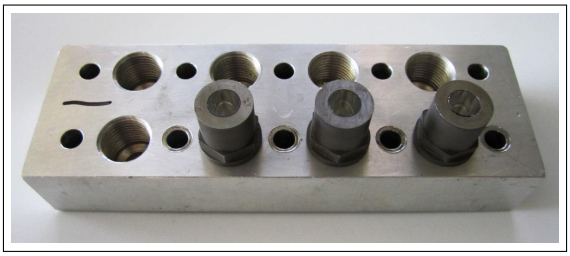

Figure 5.6: Gripper Block with 330 head-out style grippers

for interfacing any size and style of PAAW gripper to the testing system; blocks have been made to hold 250 and 330 head-out style grippers (figure 5.6). As polymerized adhesive can be time consuming to remove manually, the gripper block allows the experimenter to index a clean gripper into position rather than clean the used gripper immediately after each test. When all eight grippers have been used, the polymerized adhesive can be removed quickly by mounting the gripper block in a CNC machine tool and running an automated adhesive grinding cycle with a specially designed grinding tool (figure 5.7). Anvils may be installed in a gripper block and cleaned with the same grinding cycle.

There are five beams of varying stiffness shown in figure 5.8; from left to right in the figure, the stiffnesses are .013, .64, 15, 56, and 114 N/μm. Table 5.1 summarizes the attributes of the beams. The top surfaces have been either machined or ground to a flatness error less than .05 mm. The unsupported span of the beams is 128 mm and the approximate width is 38 mm. The beams are intended to easily slide into or out of the system between test.

The beams are supported on either end by a pair of support columns (figure 5.9). A

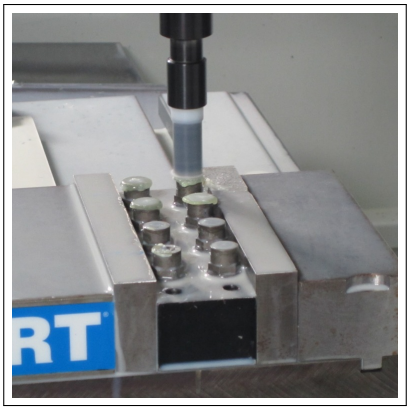

Figure 5.7: Automated adhesive removal

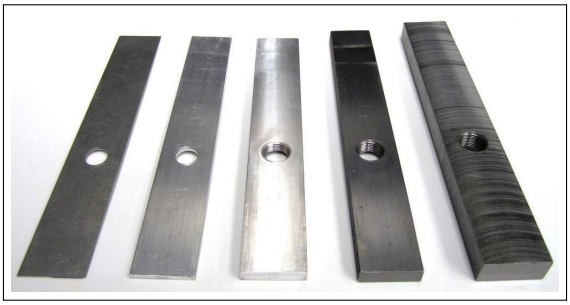

Figure 5.8: Beams of varying stiffness

set of three dowel pins inside the support columns facilitate the repeatable placement of the beam relative to the system. Two screws fasten a small clamp plate against the beam, securing it in place. Under the clamp plate, springs lightly hold the plate to the beam to ensure that it remains flush to the beam and does not pinch only one side when tightened.

The columns sit on 9125 Kistler piezo-electric force transducers (figure 5.10). With an axial stiffness of approximately 2600 N/μm, the transducers will have a negligible contribution to the overall system compliance. Piezo-electrics do, however, experience charge drain during static loading. The primary purpose of the force transducers in this apparatus is to

Table 5.1: Beam attributes

Stiffness (N/μm)	.013	.64	15	56	114
Thickness (mm)	.81	3.2	8.9	11.2	18.3
Material	6061	6061	6061	Steel	Steel

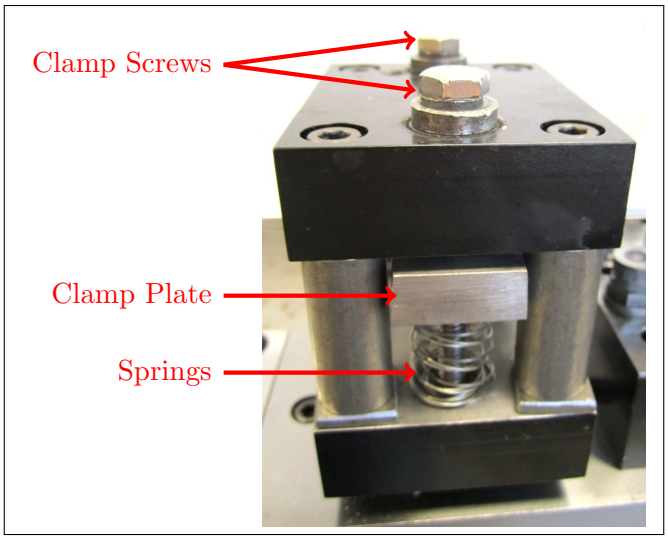

Figure 5.9: Support Column

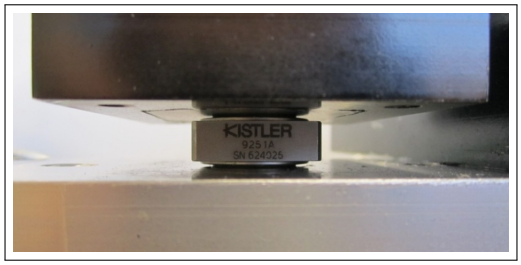

Figure 5.10: Force Transducer

accurately determine the system stiffness. For each beam, the stiffness should be repeatable and obey the ideal spring relationship: $F = k \cdot D$ where k is the spring stiffness and F and D are the force and displacement, respectively. The measured stiffness is also compared with the stiffness predicted by analytical beam models. For compliant beams, the support columns act like fixed boundary conditions; for the stiffest beam, bending of the columns must be taken into account.

In order to have repeatable and linear stiffness for the thicker beams, it is necessary to preload the anvil nuts into the beam. Without any preloading, the contact stiffness at the anvil nut beam interface is either less than or on the same order of magnitude of the stiffness of these beams. To overcome this, one set of anvil nuts have external threads which

Figure 5.11: Anvils assembled in externally threaded nuts

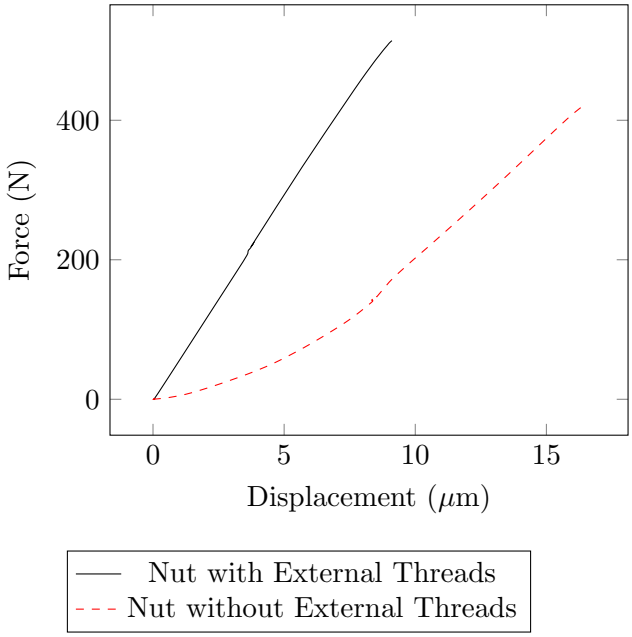

Figure 5.12: Force-displacement response of 56 N/μm beam

are used to fasten them into threaded holes in the 15, 56, and 114 N/μm beams. Figure 5.11 shows externally threaded anvil nuts for joint gaps of 2.0, 1.5, .97, and .5 mm.

Figure 5.12 shows a plot of force vs. displacement for a 56 N/μm and an anvil nut with and without external threads. Under low forces, the stiffness is governed by contact mechanics; as the load increases, the effective stiffness appears linear, but is still much less than the true stiffness of the beam.

In industrial applications featuring rigid workpieces in fixtures with closely spaced hard contact locators, it may be important to consider the effect of contact stiffness on the overall

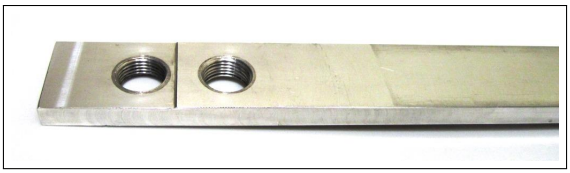

Figure 5.13: Multigripper beam

compliance of the system when predicting the amount of distortion.

5.3 Multi-gripper Hardware

The apparatus also supports experiments to test the effect of multiple grippers adhering to a workpiece simultaneously. This is done with the use of a cantilever multi-gripper beam that has two threaded holes to receive anvils (figure 5.13). The unsupported lengths at the left and right holes are 184 and 152 mm, respectively. Beam width and thickness are 38 and 9.4 mm. The top face of the beam around the left hole is machined .50 mm lower than the rest of the beam. This allows two anvil nuts of different sizes to be used to create two joints of similar thickness. For instance, using the 2.0 mm nut on the left and 1.5 mm nut on the right will produce two joints of 1.5 mm without requiring two 1.5 mm nuts.

In this configuration, shown in figure 5.14, two C30 Lion Precision capacitance gages measure displacement at each anvil. The Gripper Block mounts to the base plate under the two anvils, again using dowel pins to keep it aligned. Just like in the single gripper setup, the Gripper Block can be indexed between tests to place clean grippers in position. Straightness error of both the base plate and the multi-gripper beam has caused the gap spacing to be slightly smaller than in the single gripper setup; the differences in the left and right joint gaps are .12 and .08 mm, respectively.

To achieve another level of stiffness, the multi-gripper beam is modified by clamping it to the 15 N/μm single-gripper beam (figure 5.15). The pre-load of the clamp does not completely prevent sliding between the two beams. The experimentally derived stiffness matrices for both multi-gripper beams are shown in table 5.2.

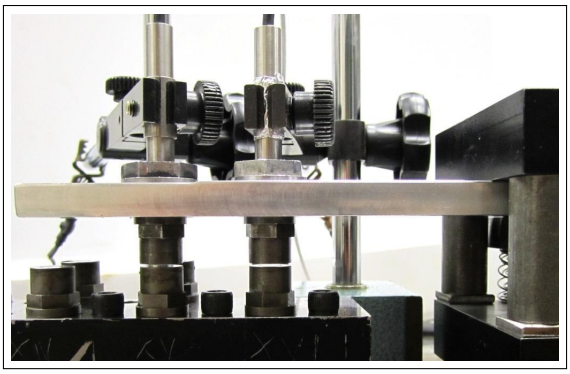

Figure 5.14: Multigripper test setup

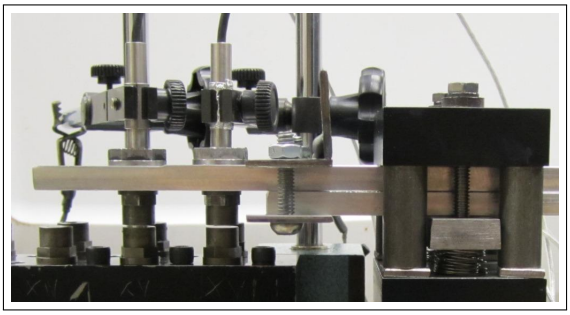

Figure 5.15: Multigripper test setup with stacked beam

The cantilever nature of the multi-gripper configuration introduces some effects not seen in the single gripper setup. The lack of symmetry may allow adhesive joints to contort the beam by applying moments in addition to axial forces.

5.4 Operation of Apparatus

Distortion experiments are performed using the following procedure:

Table 5.2: Stiffness matrices for multi-gripper beams

Multi-gripper beam

	Left	Right
Left	.40	.67
Right	.67	1.0

Stacked multi-gripper beam

	Left	Right
Left	.95	1.8
Right	1.8	2.9

Stiffness values are expressed in N/μm

1. A gripper is selected and the gripper block fastened to the base.
2. The light guide is inserted underneath the gripper.
3. An anvil is tightened into an anvil nut that is selected to produce the desired joint thickness.
4. Bonding surfaces of the anvil and gripper are cleaned with ethanol.
5. Adhesive is deposited on the gripper surface with a syringe.
6. The desired beam is installed in the system and the clamp plates are tightened.
7. The anvil nut is installed in the beam.
8. The capacitance gage is placed directly above the back of the anvil.
9. Collection of force and displacement data begins at a rate of 128 data points per second.
10. The shutter of the UV lamp opens 1-2 seconds later
11. The shutter closes after 40 seconds from the time it was opened.
12. Data collection stops at 80 seconds since it began.
13. The clamp plates are loosened.
14. The adhesive joint is broken by applying a torque on the anvil nut with a wrench
15. The experiment may be repeated with a new gripper and anvil.
16. When all grippers and anvils have been consumed, the residual adhesive is removed through an automated grinding cycle.

Figure 5.16 illustrates typical data plots obtained through a distortion test. Anvil displacement begins within a second of the shutter opening. The net displacement of the

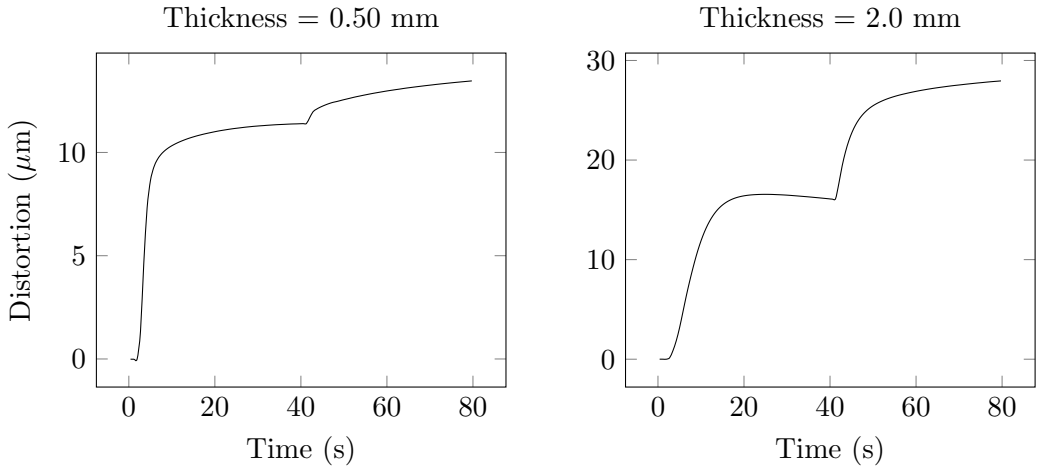

Figure 5.16: Typical distortion plots. Test conditions: 250 grippers and 15 N/μm workpiece stiffness

system approaches a saturating value within several seconds and then experiences a slight decrease as the rate of thermal expansion starts to exceed the rate of polymerization shrinkage. Heat enters the joint mainly through the absorbed high intensity radiation and to a lesser extent from the polymerization reaction. Immediately following the shutter closing, the displacement of the anvil increases sharply from thermal contraction as the adhesive joint cools.

Thicker joints tend to have a longer rise time and a more pronounced thermal contraction curve than thinner joints. The difference in rise time may be a result of two effects: a slower polymerization rate due to optical transmission losses through adhesive and a greater amount of viscous flow of the adhesive as it cures. The larger thermal curve indicates that thicker joints reach a higher peak temperature. The core region of a thick joint has a thicker layer of polymerized adhesive surrounding it to insulate it from the thermally conductive gripper and anvil which act as heat sinks. The slower response of the joint to thermal contraction is related to the time it takes for heat to escape the joint.

After the data recording stops, the adhesive may continue to experience polymerization shrinkage. After several minutes, this typically amounts to an additional displacement

of only one or two microns, which is on the same order of magnitude as the drift error sometimes observed in the capacitance gage. In this work, the total distortion is taken to be the net displacement at the conclusion of the 80 second data recording period.

Chapter 6

DISTORTION AS A FUNCTION OF WORKPIECE STIFFNESS AND ADHESIVE JOINT THICKNESS

6.1 Outline of Workpiece Distortion Experiment

One of the objectives of this work is to create a model of workpiece distortion as a function of workpiece stiffness and adhesive joint thickness. To obtain data for this model, a set of tests were performed on the single gripper test setup using 250 grippers and GB1 adhesive. The experiment consisted of five levels of workpiece stiffness (.013, .64, 15, 56, and 114 N/μm) and five levels of joint thickness (2.0, 1.5, .97, .5, and .12 mm), with two replicates at each combination of levels. The order of the tests were randomized and replicates were performed on separate days. A Dymax spot lamp with a 5 mm light guide provides 8-9 $\frac{W}{cm^2}$ of light in the UVA range. The shutter opening duration was 40 seconds and net distortion was recorded after 80 seconds from the beginning of the test.

To evaluate the robustness of the model, a set of validation data was collected using the cantilever beam distortion testing setup with the multigripper beam and the stacked multigripper beam. This experiment also included three levels of joint thickness (nominally .4, .9, and 1.4 mm) with two replicates at each combination of stiffness and thickness.

During each test, the force-displacement plot is examined for linearity and consistency with the expected stiffness. This prevents errors due to insufficient tightening from going

undetected.

6.2 Results of Workpiece Distortion Experiment

Figure 6.1 shows the effects of workpiece stiffness and joint thickness on distortion for a 250 gripper and GB1 adhesive. A model of the following form was fitted to the data.

$$D = \beta t \left(\frac{1}{1 + a t^b k^c} \right) \tag{6.1}$$

where t is the original joint thickness in mm, k is the workpiece stiffness in N/μm, β is the volumetric shrinkage percentage, and a, b, and c are model parameters. This model is unique to this work and the rationale behind it is discussed in section 6.3.

From experiments described in chapter 9, the value of β for GB1 was determined to be .067. The model parameters were found by minimizing the sum of the squared error between the measured distortion and the model prediction. For the model corresponding to the data in this experiment, a=.685, b=.789, and c=.553. The total R^2 value equals .99. The R^2 value for the validation data set is .96.

Figure 6.2 features the distortion per unit thickness, $\frac{D}{t}$, of the experimental tests. For moderate workpiece stiffness, this quantity rises sharply as joint thickness approaches zero. The maximum $\frac{D}{t}$ is the volumetric shrinkage percentage. The total R^2 values are .98 and .82 for the calibration and validation data, respectively.

6.3 Discussion of Workpiece Distortion Results

Our understanding of the effective behavior of the adhesive joint is reflected in the form of the model. The maximum possible workpiece distortion should equal the product of the volumetric shrinkage factor, β, and the initial joint thickness, t. However, as illustrated in figure 6.3, the flow of adhesive in the radial direction will reduce the net axial displacement of the workpiece. The tendency of the adhesive to pull radially inwards increases with

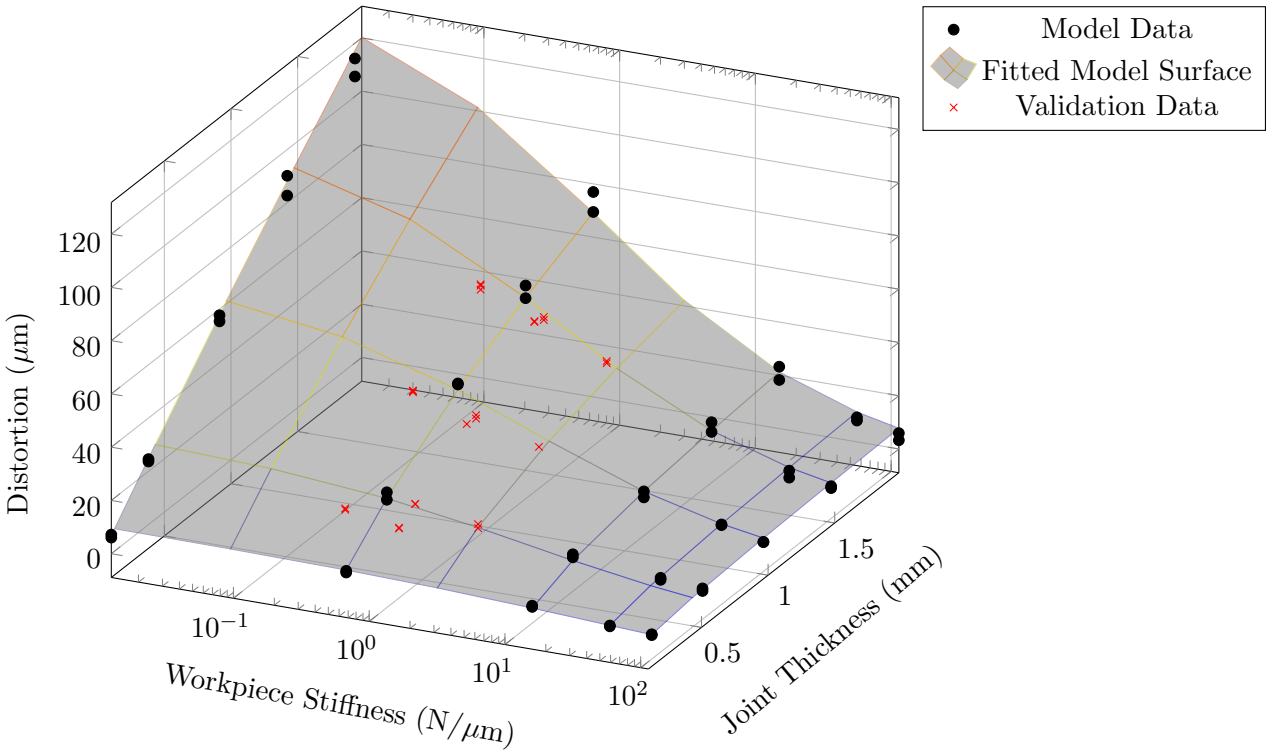

Figure 6.1: Distortion as a function of workpiece stiffness and joint thickness for a 250 PAAW gripper with GB1 adhesive

workpiece stiffness and decreases with the aspect ratio of the joint. Aspect ratio is defined as $\frac{radius}{t}$; for a given gripper geometry, the aspect ratio is a function of only the joint thickness. Since distortion will asymptotically approach zero as either the workpiece stiffness or joint thickness approaches infinity, the expression $\frac{1}{1+at^b k^c}$ was chosen to model the effect of these factors. Likewise, as either the workpiece stiffness or the joint thickness approaches zero, the distortion will approach the volumetric shrinkage factor.

Alternatively, the amount of volumetric shrinkage in the axial direction should be related to the residual force in the joint, see figure 6.4. A simple empirical model of the following form was fit to the data:

$$\frac{D}{t} = \beta \left(\frac{1}{1 + af^b} \right) \tag{6.2}$$

where f is the residual joint force in Newtons

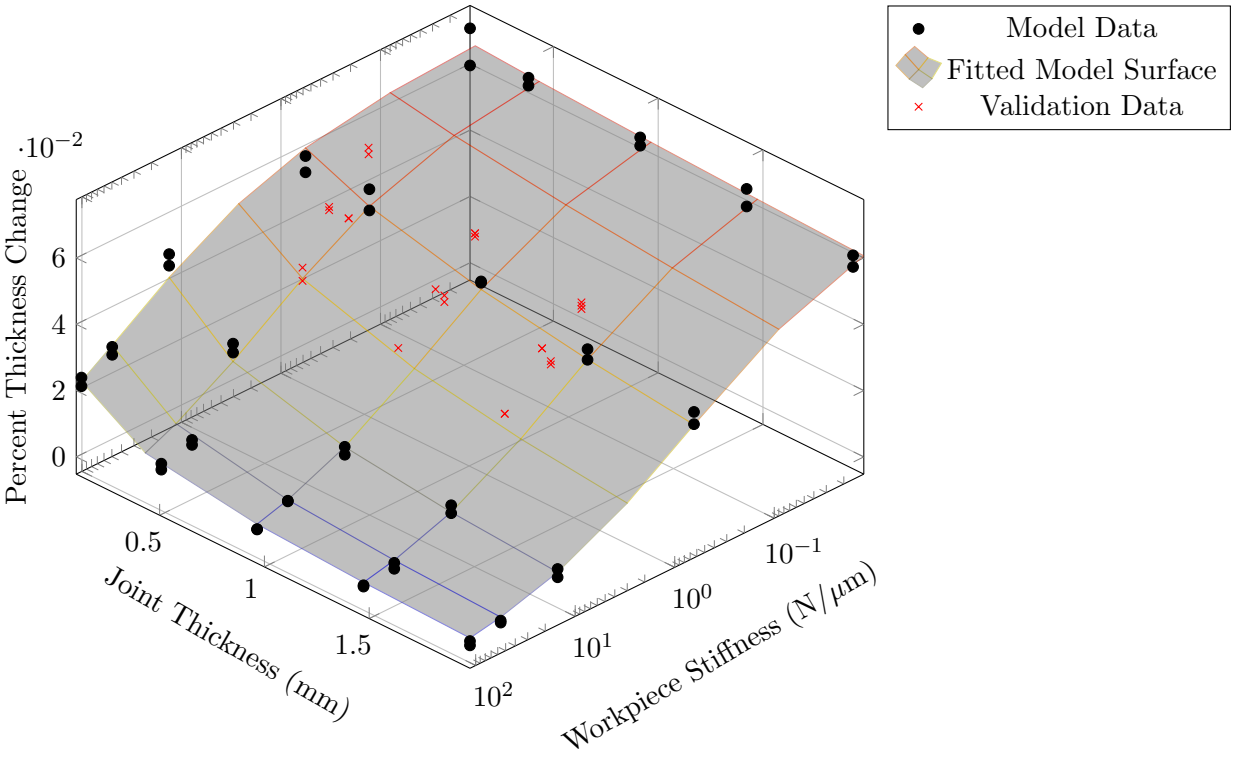

Figure 6.2: Percent thickness change as a function of workpiece stiffness and joint thickness for a 250 PAAW gripper with GB1 adhesive

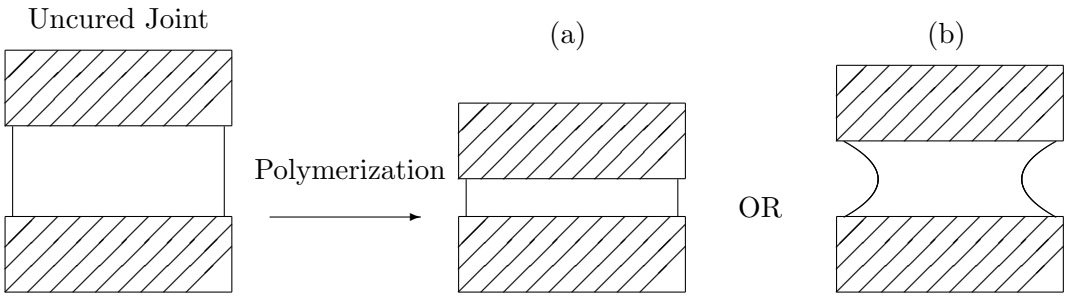

Figure 6.3: Displacement resulting from adhesive flow in the a) axial, and b) axial and radial directions

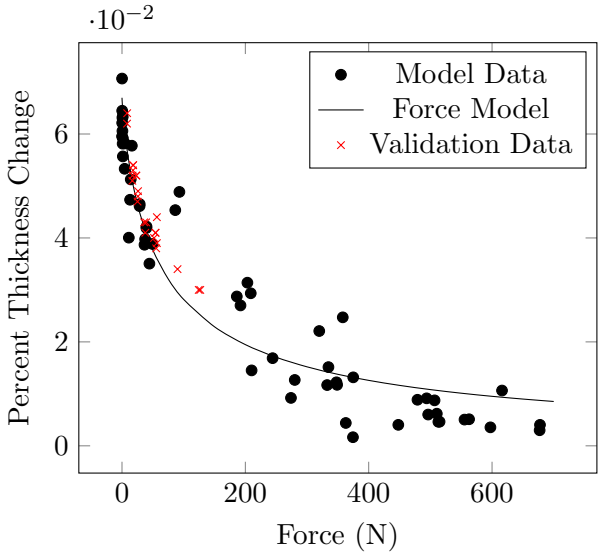

Figure 6.4: Percent thickness change as a function of residual joint force for a 250 PAAW gripper with GB1 adhesive

The total R^2 value for this model is .91. The validation R^2 value is .81.

A large force restraining the adhesive will increase the stress-induced strain and cause more adhesive to flow radially inward. Conversely, a small force should allow the joint to cure without much residual stress and facilitate shrinkage in the axial direction.

With increasing thickness, the degree of conversion of the adhesive near the workpiece may see a decline resulting from inadequate light intensity. In fact, when 2 mm thick joints are bonded to very stiff workpieces, the joint occasionally experiences a partial failure during polymerization, like the one shown in figure 6.5. This may be a result of the high stresses developing in the curing joint and a reduced degree of conversion on the far side of the joint that would leave it unable to withstand the stress and either plastically deform or initiate a crack at the interface with the anvil.

In addition, 1.5 and 2 mm joints frequently break cleanly from the anvil surface when they are destroyed in shear following the test, indicating an adhesive failure at that interface rather than a cohesive one. On the other hand, joints with thicknesses of 1 mm or less tend to break cohesively. An adhesive failure mode on the anvil side may be a sign that the light

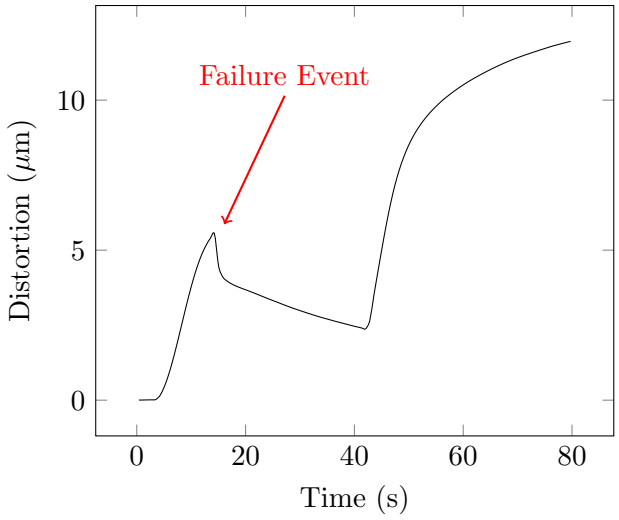

Figure 6.5: Distortion plot with partial joint failure. Test conditions: 330 gripper, 1.5 mm joint, and 56 N/μm workpiece stiffness

intensity reaching the anvil surface has diminished to the point that the degree of conversion is affected. Since volumetric shrinkage is related to degree of conversion, this may account for some of the reduction in distortion per unit thickness of larger joints.

Chapter 7

EFFECTS OF JOINT DIAMETER AND CURING CYCLE

This chapter aims to take a closer look at how the UV light intensity distribution inside a PAAW joint affects the overall workpiece distortion caused by that joint. To do this, the effects of adhesive joint diameter, gripper window diameter, and curing cycle are investigated.

7.1 Support Column Hypothesis

When the light intensity exceeds a critical value, the adhesive will polymerize at its fastest rate. Any increase in intensity above the critical irradiance will have no effect on the reaction kinetics, not considering the indirect effects associated with the corresponding increase in temperature [5]. The region in the adhesive joint where the light intensity is above the critical value is referred to in this work as the *primary cure zone*. All other regions of the adhesive joint are in the *secondary cure zone*. Figure 7.1 shows the distinction between these two zones. Since the light intensity generally decreases most quickly as the radial distance from the sapphire window increases, the primary zone can be approximated as a disc centered about the gripper's window. The size of this disc is a function of the window diameter, the joint thickness, and the light intensity entering the gripper window.

The effect of joint thickness on secondary curing has been observed in adhesives with low

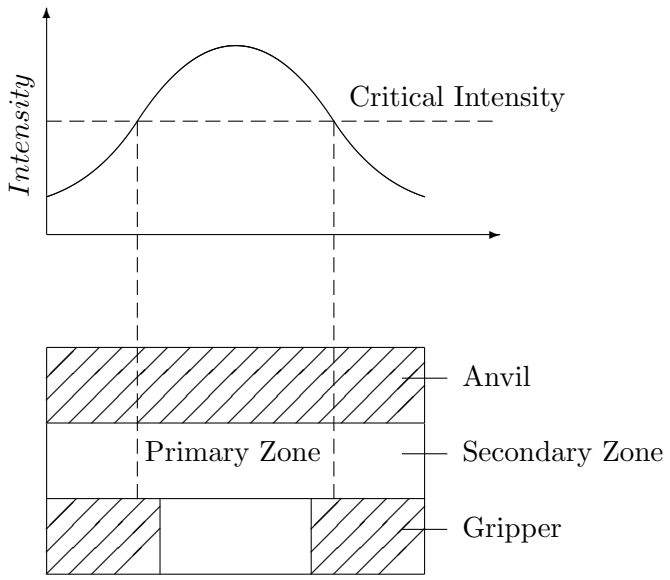

Figure 7.1: Primary and secondary cure zones

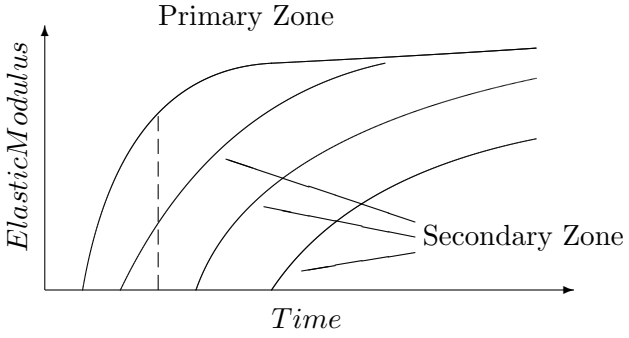

Figure 7.2: Elastic modulus development of curing zones

concentrations of photoinitiators. A smaller joint thickness results in a wider unpolymerized region along the perimeter of the gripper chassis. This effect also appears in all adhesives for joint thicknesses less than .1 mm.

The primary zone will polymerize as one unit. Adhesive in the secondary zone will polymerize at a slower rate, which is a function of the light intensity distribution. It is hypothesized that when the primary cure zone develops a substantial elastic modulus, the

adhesive in the secondary cure zone is still largely viscous, as illustrated in figure 7.2. When the secondary zone adhesive begins to develop its elastic modulus, the primary zone may act like a support column and resist any further displacement of the workpiece relative to the gripper. If this is the case, the size of the secondary cure zone should have little effect on the net axial shrinkage of the joint. The size of the primary cure zone would dictate the total amount of workpiece distortion.

However, it should be noted that both primary and secondary zones contribute to overall joint strength, which explains the design decision to make the gripper chassis's much larger than then window. The secondary zone experiences a substantial degree of conversion, although it may not be the same as in the primary zone.

7.2 Outline of Joint Diameter Experiment

To test the support column hypothesis, an experiment was performed where the sizes of the primary and secondary cure zones were varied. The experiment features two levels of gripper window diameter, 6.35 and 8.38 mm, to set the maximum primary zone size. The adhesive joint diameter was continuously varied from 4.5 to 12.5 mm for the 250 gripper and 4.5 to 15.5 mm for the 330 gripper. A 1.4 mm nominal joint thickness was used to provide sufficient contrast for the effect of the primary and secondary cure zones. Joints thinner than 1.4 mm have a large ratio of experimental variation to measured distortion which makes perceiving a trend difficult. Three levels of beam stiffness, .013, .64, and 56 N/μm, were selected for this experiment to show whether there is an interaction effect with workpiece stiffness and joint diameter.

The diameter of the adhesive joint is difficult to control, so the following method was used: A droplet of adhesive is deposited on the center of the gripper window. After lowering the anvil through the beam, the anvil is turned one full rotation in an effort to improved the concentricity of the adhesive disc about the gripper window. After the test has finished, the joint is broken with care and its diameter is measured with digital calipers that have a

Figure 7.3: Measurement of adhesive joint diameter

resolution of .01 mm (see figure 7.4). The average of the largest and smallest measurements is recorded. The total range of the measured diameters is typically .1 to .6 mm. The outer walls of the plastic joint are concave, with a diameter in the middle on the order of .2 mm less than the diameter at the gripper or anvil surface. All caliper measurements are taken along the gripper or anvil surface.

7.3 Results and Discussion of Joint Diameter Experiment

Figure 7.4 shows the resulting workpiece distortion as a function of adhesive joint diameter for two levels of sapphire window diameter and three workpiece stiffnesses. The fitted line for the 56 N/μm stiffness has the equation, $D = 1.13d - 4.37$, where D is the distortion in μm and d is the joint diameter in mm.

The results performed with the .64 N/μm beam support the notion of a development of a support column that resists further axial shrinkage from the secondary zone. For both gripper window sizes, the increasing size of the secondary zone beyond the window diameter adds little to the net axial distortion. The size of the primary zone more or less dictates the total amount of distortion. When the adhesive joint is entirely in the primary zone, the sapphire window size appears to cause only a minor difference in workpiece distortion.

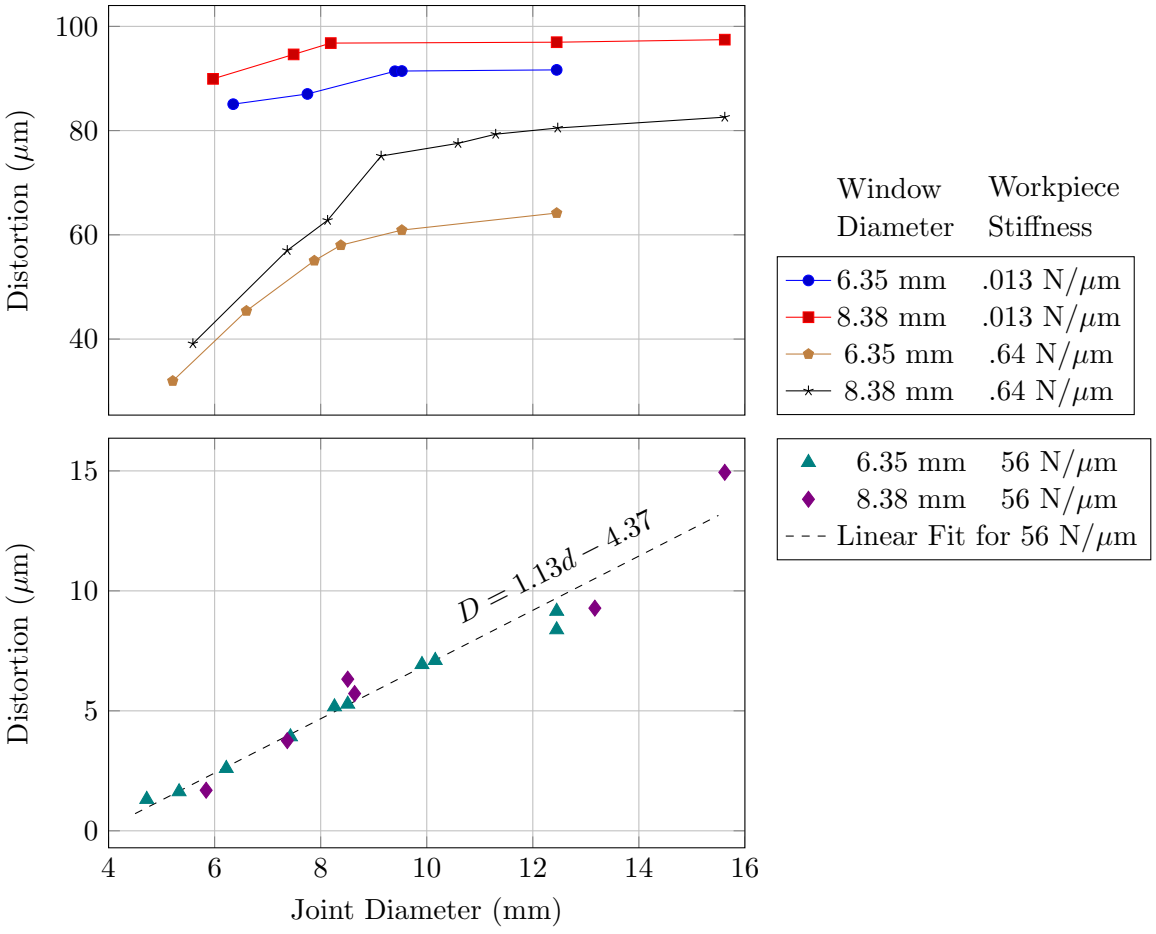

Figure 7.4: Effect of joint diameter, window diameter, and workpiece stiffness on axial distortion with 1.4 mm joint thickness

The 330 gripper uses an 8 mm light guide which provides approximately the same light intensity to the adhesive joint as the 5 mm light guide. It is possible that a difference in intensity may account for slight increase in the primary zone distortion of the 330 grippers at low workpiece stiffnesses.

For large workpiece stiffnesses, the plot of distortion vs. joint diameter does not level off. Rather, the distortion continues to increase linearly all the way until the joint diameter reaches the perimeter of the gripper chassis. In this case, there is no clear distinction between the primary and secondary cure zones in terms of contribution to workpiece distortion.

Interestingly, the relationship appears linear and not second order polynomial. Naively,

one would expect the force generated by the adhesive contraction to be proportional to the bonding area of the joint, which increases with square of the diameter. The first adhesive to cure may provide some resistance against further deformation, but this is insufficient to counteract the force of the adhesive curing in the outer regions. With large workpiece stiffness, the contraction strain and therefore the stress is much higher. Furthermore, the stiffness of the workpiece greatly exceeds the stiffness of the polymerized primary zone. As a result, the initial cured region has only a moderate effect on reducing distortion.

There does not appear to be any significant difference in this behavior between the 250 and 330 grippers for high stiffness workpieces. It is expected that the coefficients of the fitted line would depend on both joint thickness and workpiece stiffness.

The tests with the 8.38 mm window and .013 N/μm beam approach a saturation value of distortion very quickly with increasing joint diameter. Since the diameter to thickness ratio of the region above the sapphire is 6 and the residual force is only 1.2 N, it is believed that these tests, with joint diameter greater than 8 mm, experience pure axial shrinkage. In chapter 9, these test conditions are used to estimate the volumetric shrinkage factor of adhesives.

7.4 Soft Start Cure Cycle

A related concept is the soft start curing strategy that is commonly employed for reducing residual stresses and distortion in adhesive joints. A soft start curing cycle consists of initially exposing the adhesive to a small amount of radiation, waiting for the initial reaction to complete, and then exposing the adhesive to a typical dose of radiation to fully cure it. The theory behind a soft start cure is that the initial exposure will cause the joint to begin polymerizing at a reduced rate. The reduced rate gives the adhesive plenty of time to viscously flow and relieve some of the accumulating shrinkage stresses. In addition, the adhesive directly in front of the UV light source will polymerize to a much greater extent than the surrounding adhesive during the initial exposure. In a PAAW system, this may

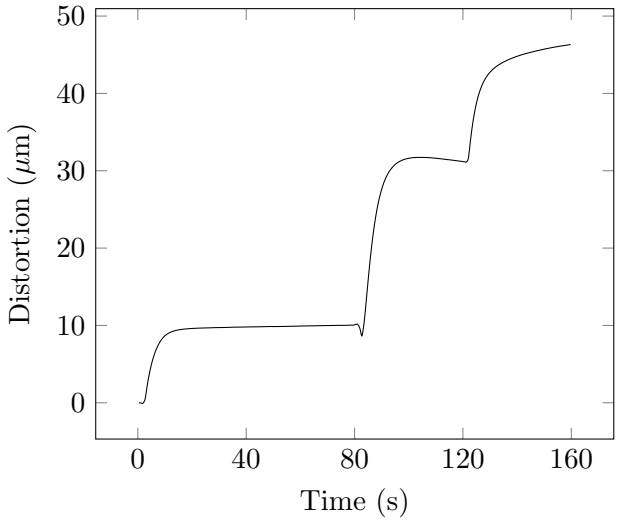

Figure 7.5: Distortion from soft start curing cycle with 1.5 mm joint and .64 N/μm workpiece stiffness

enhance the effect of the primary zone support column.

To test this idea, the following experiment was performed: The adhesive is initially exposed for 1 second with 8 W/cm^2 UVA intensity. At the conclusion of 80 seconds, the joint is exposed at with the same intensity for 40 seconds. Distortion is measured after 160 seconds. Figure 7.5 shows the resulting distortion plot.

With two replicates, the total distortion ranged from 43 to 46 μm. The conventional curing approach with the same workpiece stiffness and joint thickness caused 57 to 62 μm of distortion. Thus, the soft start method reduced distortion by 25%.

Some further experimentation is necessary to determine the optimal light intensity and exposure time to minimize distortion. These parameters will very likely be a function of the workpiece stiffness and joint thickness.

The time required between initial exposure and the second exposure only needs to be slightly greater than the time it takes the initial reaction to slow down. In the case of a 1 second initial exposure to a 1.5 mm joint, this time appears to be approximately 10 seconds.

Following the initial exposure, the adhesive in the secondary zone showed no signs of

polymerization, so the majority of the initial polymerization must have occurred in the primary zone.

Chapter 8

MULTIJOINT DISTORTION ANALYSIS

The previous chapters summarized investigations on the response of a symmetric workpiece to an individual PAAW joint bonding to its center. However, most PAAW implementations will hold the workpiece with more than one PAAW joint in a non-symmetric configuration.

There are two ways the set of adhesive joints in a PAAW system can be cured: simultaneously or sequentially. A simultaneous cure involves using either multiple lamps or light guides with multiple output ends to cure all of the joints at the same time. Sequential curing, also known as incremental curing, refers to the process of polymerizing each individual joint of the an adhesive system one at a time. From an industrial standpoint, sequential curing increases process cycle time and decreases operator productivity. However, a carefully designed sequential curing strategy can reduce workpiece distortion at critical locations and adhesive joint residual stress.

The adhesive joint curing order has a large effect on the resulting distortion and residual stress accumulation in the system. Each polymerized joint adds a support condition to the workpiece, altering the stiffness matrix of the system. Fortunately, the final outcome can be predicted by considering the response of each adhesive joint at each step of the curing sequence.

The objective of this chapter is to shed light on the effects of curing multiple grippers to a workpiece and present a method of predicting the resulting distortion.

8.1 Outline of Multigripper Experiment

Distortion experiments were performed on the cantilever multigripper beam and the stacked version of that beam (see figures 5.14 and 5.15). The gripper furthest from the support column will be referred to as "gripper 1" and the gripper closer to the column as "gripper 2". The stiffness matrices of the two beams were derived from the force-displacement plots of adhesive joints curing on either gripper 1 or gripper 2; these matrices are found in table 5.2. Three levels of nominal joint thickness were investigated: .4, .9, and 1.4 mm. Due to slight parallelism error of the test apparatus, the gap thickness of gripper 1 is .05 mm smaller than the thickness of the joint on gripper 2.

Four cases were explored:

- Cure joint 1 only
- Cure joint 2 only
- Both joints cured simultaneously
- Joint 1 cured first followed by joint 2 (Sequential cure)

To perform a simultaneous cure, two spot lamps were used. Gripper 1 is connected with a 5 mm light guide to the Dymax lamp and gripper 2 is connected to the Omnicure lamp. The Dymax and Omnicure lamps output an intensity of 7-9 $\frac{W}{cm^2}$ and 5-6.5 $\frac{W}{cm^2}$ in the UVA range, respectively. This difference in intensity is not expected to have a significant effect. This assumption was verified with several preliminary experiments with the lamp positions switched. All other tests used the Dymax lamp exclusively.

The sequential cure experiments all involve curing joint 1 first. The reason for this is that bonding joint 2 alone leads to as much or more distortion than curing both joints simultaneously for all levels of joint thickness and workpiece stiffness. Since it is desirable to minimize distortion, there is no practical advantage to curing gripper 2 first.

As with the other distortion experiments, the exposure time is 40 seconds and the data acquisition ends at a total elapsed time of 80 seconds. 250 style grippers and anvils were used. Two replicates were performed for each combination of levels at each of the four cases. One important difference between this experiment and the single gripper experiments is that the lack of symmetry in the cantilever beam configuration allows rotation of the anvils and moment loading on the anvil from the joint.

8.2 Results and Discussion of Multigripper Experiment

Figure 8.1 presents the results of the multigripper experiments. In most cases, a simultaneous cure leads to less overall distortion of the workpiece than curing gripper 2 alone. The joint on gripper 1 develops a significant elastic modulus during the cure to resist the motion of the beam that would have been caused by joint 2 curing. This effect is much more pronounced for thin joints. Larger joints deform the workpiece more and consequently experience greater resistive forces which causes more radial adhesive flow during polymerization. However, two joints working together will divide the beam's resistance, reducing the amount of radial flow while increasing the relative distortion somewhat.

From these results, it appears that a sequential cure is capable of minimizing the distortion at any one location. The sequential cure distortion at gripper 1 was less than or equal to the simultaneous cure distortion in all tests. However, for the stiffer workpiece, using a sequential cure resulted in the most distortion at gripper 2.

It is clear that in a simultaneous cure, the net distortion is not equal to the linear sum of the distortions caused by the individual joints acting alone. This interaction presents great challenges to creating a predictive model for this type of curing. The nature of the interaction between grippers is a function of reaction rate, the stiffness matrix of the system, and the thickness of the joints. On the other hand, sequential cures are relatively easy to model since the effects of each joint can be calculated independently and added together to yield the total distortion. This is discussed in detail in the next few sections.

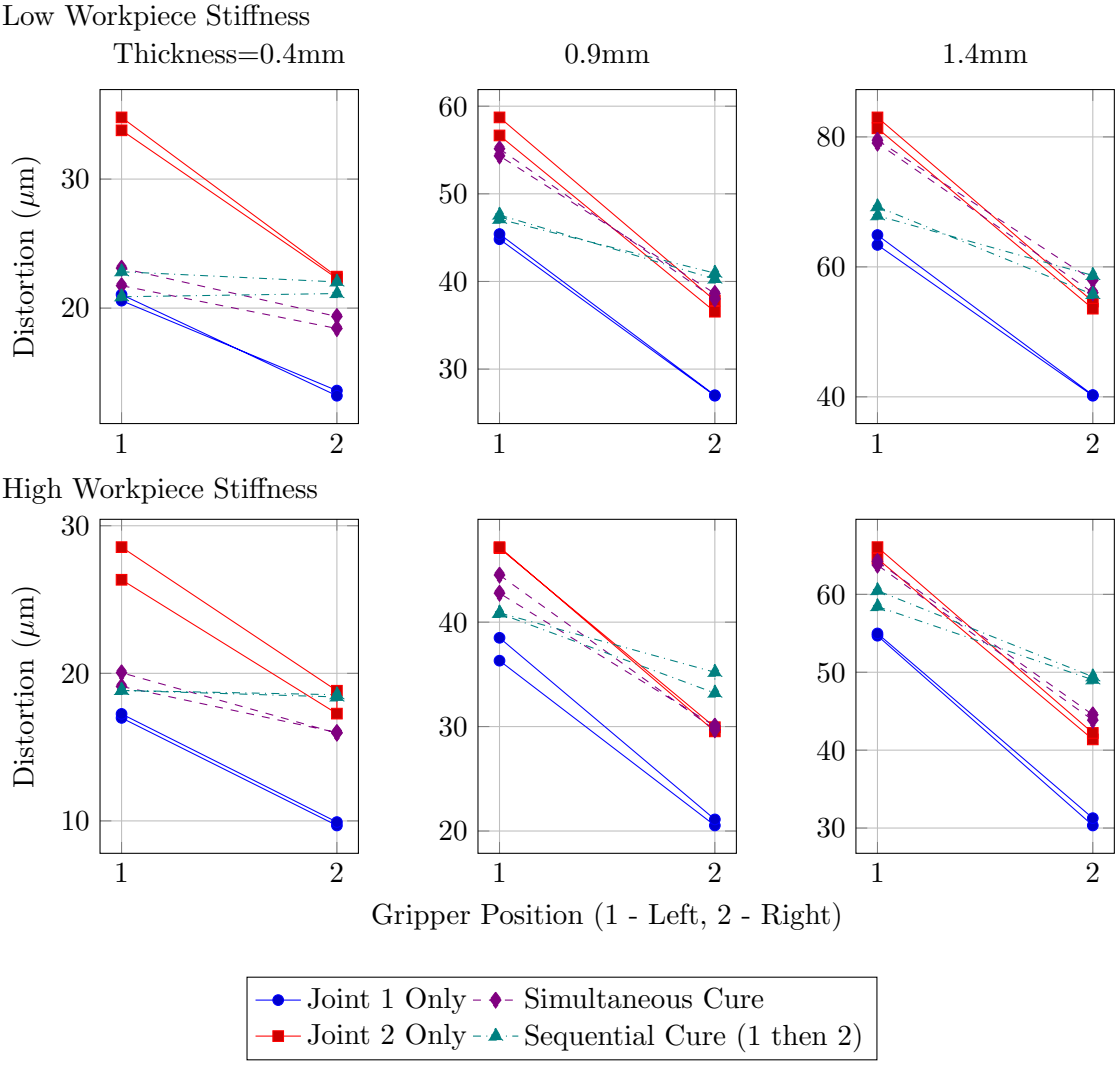

Figure 8.1: Workpiece distortion with two grippers at varying levels of workpiece stiffness, joint thickness, and curing sequence

8.3 Predicting Sequential Cure Distortion

The workpiece distortion created in sequentially cured PAAW systems can be predicted with reasonable accuracy using the method discussed in this section. A short case study of a sequential cure on the multigripper distortion test is presented alongside the solution methodology.

First, it is helpful to consider the distortion of various locations in the workpiece in

terms of a vector, defined in this work as the "distortion vector" or "state", D.

$$D_i = \begin{bmatrix} d_{i,1} & d_{i,2} & \cdots & d_{i,n+m} \end{bmatrix}^T \tag{8.1}$$

Each $d_{i,j}$ represents the distortion at the j^{th} location after the i^{th} step in the sequence. n is the number of grippers and m is the number of critical locations not above a gripper. The initial distortion state, D_0, is a vector of zeros by definition. Determining the final state, D_n, is the objective of the analysis.

Distortion may be predicted by considering the grippers one at a time. For each gripper, the amount of distortion at this gripper can be computed using a model similar to the one derived in chapter 6. Each cured joint will act like a support and change the stiffness matrix of the workpiece. These joints will also alter the distortion state of the workpiece. The new workpiece stiffness and distortion state must be taken into account to predict the distortion at each subsequent gripper.

The stiffness matrix of the fixtured workpiece, K, may be expressed as follows:

$$K_i = \begin{bmatrix} k_{i,1,1} & k_{i,1,2} & \cdots & k_{i,1,n+m} \\ k_{i,2,1} & k_{i,2,2} & \cdots & k_{i,2,n+m} \\ \vdots & \vdots & \ddots & \vdots \\ k_{i,n+m,1} & k_{i,n+m,2} & \cdots & k_{i,n+m,n+m} \end{bmatrix} \tag{8.2}$$

Each $k_{i,j,j\prime}$ represents the ratio of normal force applied to location j and the resulting normal displacement of location $j\prime$. Like all structural stiffness matrices, it is symmetric. Off-diagonal terms are referred to as the cross stiffness values.

K_i must be determined for $i = 0...n$ using either analytical or numerical methods. The rows in the matrix corresponding to joints that have already been cured do not need to be computed. The distortion on the workpiece caused by curing a single joint can be superimposed on the previous distortion state.

Knowing K_i, the joint thickness, and the distortion model parameters, D_{i+1} can be

determined as follows, where g is the gripper being cured during step $i+1$.

The distortion introduced at the individual joint can be computed from the empirical model of chapter 6:

$$d_{i+1,g} - d_{i,g} = \beta t_g \left(\frac{1}{1 + a t_g^b k_{i,g,g}^c} \right) \tag{8.3}$$

The residual force, F_g, at that joint can be computed from the stiffness:

$$F_g = k_{i,g,g} \left(d_{i+1,g} - d_{i,g} \right) \tag{8.4}$$

From the force and stiffness matrix, the change in distortion at all locations can be found:

$$D_{i+1} - D_i = F_g \left[\begin{array}{cccc} \frac{1}{k_{i,g,1}} & \frac{1}{k_{i,g,2}} & \cdots & \frac{1}{k_{i,g,n+m}} \end{array} \right]^T \tag{8.5}$$

Combining the above equations, equation 8.6 can be derived:

$$D_{i+1} = D_i + \left[\beta t_g \left(\frac{1}{1 + a t_g^b k_{i,g,g}^c} \right) \right] k_{i,g,g} \left[\begin{array}{cccc} \frac{1}{k_{i,g,1}} & \frac{1}{k_{i,g,2}} & \cdots & \frac{1}{k_{i,g,n+m}} \end{array} \right]^T \tag{8.6}$$

Note that joint thickness, t_j, is not a function of sequence step in equation 8.6. While the thickness does change as a result of distortion, the change in thickness is typically less than 5% of the original thickness. If the joint thickness changes significantly for a particular setup, it can be calculated as follows:

$$t_{i,j} = t_{0,j} - d_{i,j} \tag{8.7}$$

It is necessary to know the joint thickness a priori. In applications where joint thickness is highly variable, the designer may consider which combination of joint thicknesses will yield the greatest distortion at the critical features.

Determining the joint curing sequence requires knowledge of the critical tolerances and a general understanding of how the workpiece will distort in response to each joint. The

following simple rules can be used to select a curing sequence:

- Select the joints that have small ratios of direct stiffness to cross stiffness of the critical regions
- Use joints near critical features as supports to resist further distortion at these locations

If hard contact locators are situated between two grippers, one gripper may pull the workpiece away from the other gripper when it cures. Curing the second gripper may result in a net distortion near zero. Careful consideration is required in these cases.

For complex workpieces and configurations, it may be wise to automate the stiffness matrix determination process and perform a brute force search of all possible curing sequences.

8.3.1 Modeling a PAAW system

The stiffness matrix of the system at each step in the solution process can be determined computationally through a Finite Element (FE) analysis.

When creating an FE model, there are a number of options on how to simplify the system to save memory, computational time, and model building time. The modeler must first decide how to represent each of the following aspects of the system:

- Workpiece
- Clamps and locating elements
- Fixture
- Previously cured adhesive joints

The workpiece no doubt should be modeled as a deformable material. The choice of element type depends on the workpiece geometry. Clamps and locators may be modeled as

deformable solids, rigid solids, or simply as boundary conditions applied to the workpiece depending on the relative amount of elastic deformation they experience and the nature of their contact with the workpiece. Complete fixtures may not be necessary to model as they are typically designed to be much more rigid than the workpiece. However, if the fixture undergoes considerable elastic deformation during the joint curing, it should be modeled with deformable elements. Modeling of previously cured joints is discussed below in section 8.3.3.

Each row in the stiffness matrix is determined by applying a load to the workpiece directly above a gripper and measuring the resulting displacement at all of the critical locations. For gripper j in solution step i, $k_{i,j,j\prime}$ is equal to the total applied force divided by the displacement of a point at location $j\prime$. If distortion of this location is more critical in one particular direction, then use the projected displacement of the point along the critical direction. Section 8.3.2 discusses appropriate ways of modeling the applied load.

Figure 8.2 shows a meshed FE model of the entire multigripper distortion test configuration created with the ABAQUS software package. Since the gripper block and base plate exhibit negligible bending, it is not necessary to include them in the model as deformable solids. The revised model is shown in 8.3. The two columns remain since their bending has a significant effect on the overall stiffness of the system. The bottom surface of the force transducer models have a fixed boundary condition. Simulation results of the original model of the entire system and the simplified model yield identical stiffness matrices.

8.3.2 Modeling Polymerization Contraction Loading

There are four general approaches for modeling the contraction of a polymerizing adhesive joint:

- Concentrated force
- Pressure distribution over the contact patch

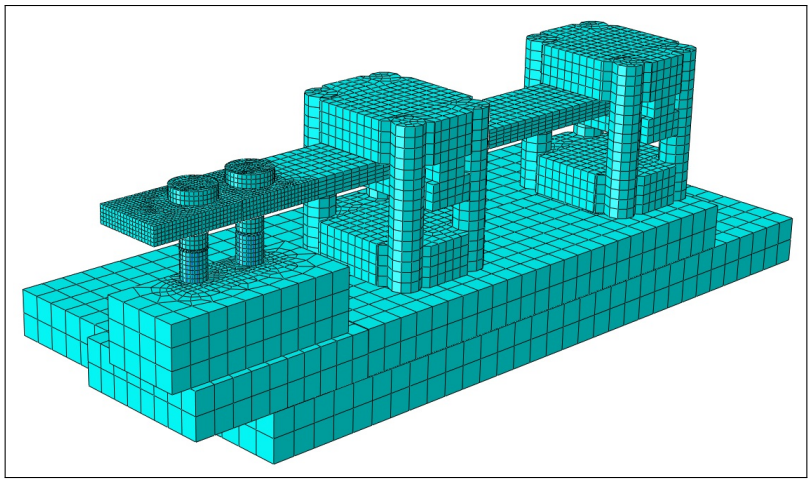

Figure 8.2: Finite Element model of workpiece, adhesive joint, and fixture

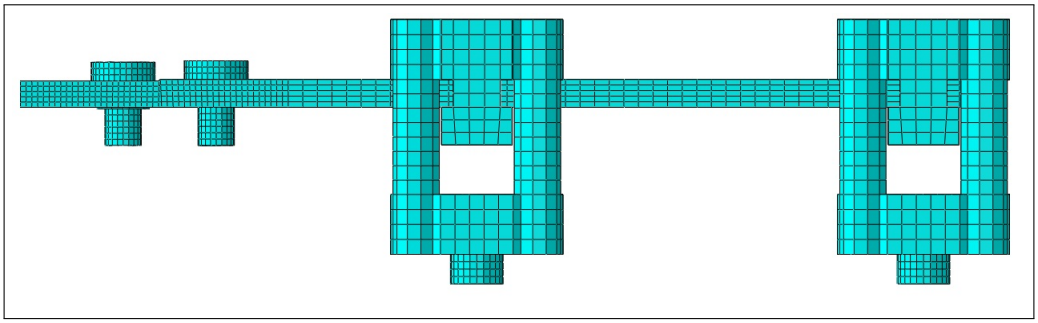

Figure 8.3: Finite Element model of workpiece and compliant components of the fixture

- Displacement of the contact patch
- Temperature displacement of a deformable solid

The simplest method of modeling a curing joint is a concentrated force acting along the axis of the gripper. This works well when the stiffness of the workpiece at and around the contact patch is sufficient to prevent significant shape distortion in response to the adhesive contraction. What is considered significant is application specific.

The second approach would potentially be the most accurate method and especially useful for workpieces with thickness less than 1mm. However, no models exist for describing the pressure distribution over the contact patch of a curing PAAW joint.

Alternatively, contraction loading on thin workpieces can be modeled as a displacement condition where either a subset of or the entire contact patch moves a fixed distance. This would only be appropriate when the local bending resistance of the workpiece is small.

The last approach, a change in temperature of a deformable solid, is commonly used in the literature for predicting stress distributions in a polymerized adhesive. The method involves creating a solid model of an adhesive joint with the elastic modulus of the adhesive when fully polymerized and a volumetric coefficient of thermal expansion equal to the volumetric polymerization shrinkage. The temperature of the joint is displaced downwards by one temperature unit.

The total axial force through the joint and the resulting displacement at each of the workpiece locations would be used to compute one row of the stiffness matrix. If the force-displacement behavior is nonlinear, a linear fit of the data should be obtained for displacements of the curing joint ranging from 0 to βt_{joint}.

Note that when modeling the fixture with deformable elements, it is important to apply a load on the gripper whose net force is equal and opposite to the load applied on the workpiece.

The case study uses a concentrated force because the local stiffness at the anvil bonding surface is large. In other words, the shape distortion of the anvil is very small compared to the displacement at this location caused by bending of the whole the workpiece.

8.3.3 Modeling Existing Joints

The previously cured adhesive joints could either be modeled as a deformable solid or simplified boundary conditions applied to the workpiece surface. The decision will depend on the relative axial and bending stiffnesses of the joint compared to the stiffness of the workpiece.

Modeling the adhesive joint as a deformable solid will provide the highest fidelity at the cost of additional modeling time. Although the elastic modulus of a joint may not

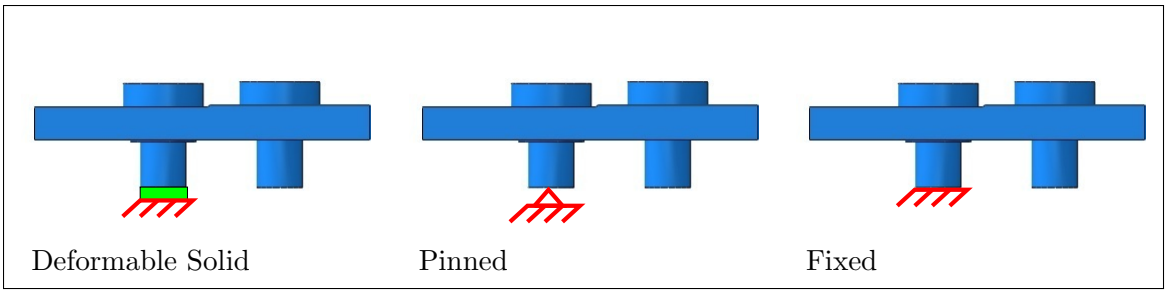

Figure 8.4: Modeling approaches for modeling existing adhesive joints

necessarily be uniform throughout, it may be acceptable to model the joint as a solid of uniform modulus with a diameter equal to or slightly greater than the gripper chassis diameter. Two common boundary conditions may be used to model the effect of an existing joint. The pinned condition prevents translation of a single point on the workpiece directly above the center of the gripper. The fixed condition restricts both translation and rotation of all the nodes on the contact patch of the adhesive joint. The diameter of the contact patch of a fixed condition that would best emulate a real adhesive joint is a complicated issue deserving of some further investigation. For practical purposes, however, it may be sufficient to use the same diameter as the gripper chassis. Figure 8.4 illustrates these three modeling approaches.

To evaluate the fidelity of these modeling approaches, simulations were performed on the finite element model of the system and compared with the experimentally measured system stiffness.

The actual stiffness of the system was determined experimentally by curing adhesive joint 1 on the left anvil and hanging known weights from a cable adhered to location 2, the center point of the right anvil bonding surface. Figure 8.5 shows the force-displacement curves of location 2 for a variety of joint 1 thicknesses. This particular system's stiffness is relatively insensitive to the thickness of joint 1.

Table 8.1 lists the values of right anvil stiffness, $k_{1,2,2}$, and left anvil cross stiffness, $k_{1,2,1}$, determined through different modeling approaches. In all approaches, a 100 N load was

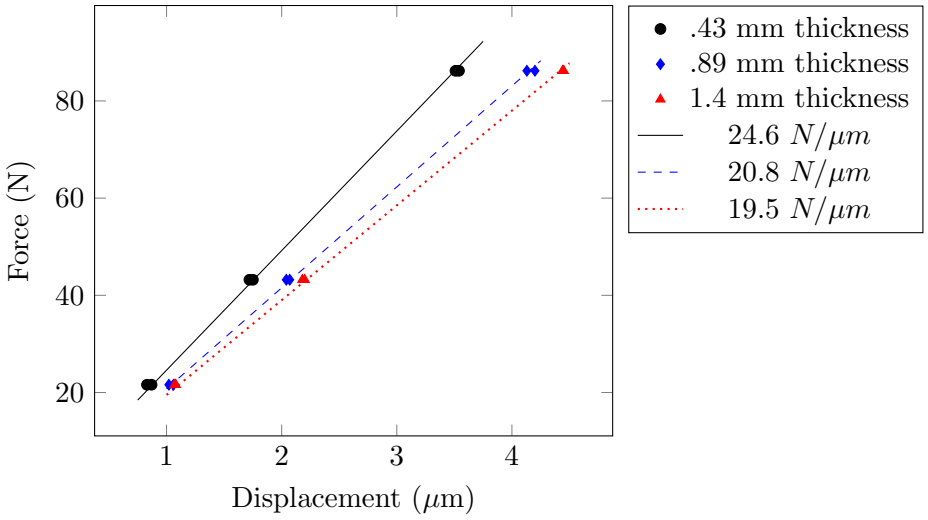

Figure 8.5: Force-Displacement plots of location 2 with varying joint 1 thickness

Table 8.1: Comparison of adhesive joint models for a 1.4 mm joint on gripper 1

Modeling Approach	$k_{1,2,2}$ $(N/\mu m)$	$k_{1,2,1}$ $(N/\mu m)$
Deformable Solid	20.3	72.3
Pinned	19.1	40.7
Fixed	39.0	1797
(Experimental)	19.5	22.7

applied to the center point of the right anvil's bonding surface. The vertical displacements of the center point of the top surface of both anvils were recorded. This was done to mimic the capacitance gage reading in the physical test apparatus setup.

The deformable solid model of a 1.4 mm adhesive joint results in an estimate of $k_{1,2,2}$ that is very close to the experimentally measured stiffness. The pinned boundary condition also yields a very good estimate for this particular workpiece. The fixed condition greatly overestimates the effective stiffness. While adhesive joints offer some moment resistance, they cannot prevent rotational distortion. It is possible that a fixed boundary condition would be suitable in other situations, such as a workpiece with a thickness on the order of 1 mm.

The cross stiffness of the cured joint, $k_{1,2,1}$, is not particularly useful since the amount

of further distortion experienced by the existing adhesive joint as a nearby joint cures is usually on the order of a few micron. Note that the cross stiffness is not infinite for the pinned and fixed boundary conditions. Although pinned and fixed boundary conditions prevent translation in the vertical direction, the displacement is measured at the top of the anvil, and elastic deformation or rotation of the anvil will cause the top node to translate vertically relative to the node(s) at the boundary condition. Furthermore, the cross stiffness experimentally measured does not necessarily reflect the motion of the left anvil as joint 2 is cured. A curing joint may create some moment loading rather than pure axial loading.

8.3.4 Results of Sequential Cure Case Study

With the values of the stiffness matrices derived from the FE models, it is possible to predict the distortion of the system in the case study. The solution steps are presented below. The joint created at the conclusion of step 1 was modeled as a deformable solid.

Step 0: Initial system

$$D_0 = \begin{bmatrix} 0 \\ 0 \end{bmatrix} \qquad K_0 = \begin{bmatrix} .40 & .67 \\ .67 & 1.0 \end{bmatrix} N/\mu m \qquad t = \begin{bmatrix} 1.35 \\ 1.40 \end{bmatrix} mm$$

Step 1: Cure joint 1

$$D_1 = D_0 + \left[.067 \cdot 1.35 \cdot \left(\frac{1}{1 + .685 \cdot 1.35^{.789} .40^{.553}}\right)\right] .40 \begin{bmatrix} \frac{1}{.40} \\ \frac{1}{.67} \end{bmatrix} = \begin{bmatrix} 59.4 \\ 35.5 \end{bmatrix} \mu m$$

$$K_1 = \begin{bmatrix} -- & -- \\ 72.3 & 20.3 \end{bmatrix} N/\mu m$$

Step 2: Cure joint 2

$$D_2 = D_1 + \left[.067 \cdot 1.4 \cdot \left(\frac{1}{1 + .685 \cdot 1.40^{.789} 20.3^{.553}}\right)\right] 20.3 \begin{bmatrix} \frac{1}{72.3} \\ \frac{1}{20.3} \end{bmatrix} = \begin{bmatrix} 64.0 \\ 51.9 \end{bmatrix} \mu m$$

Table 8.2: Comparison of predicted and measured sequential cure distortion

Step 1	$D_{1,1}$ (μm)	$D_{1,2}$ (μm)
Predicted	59.4	35.5
Replicate 1	65.4	37.5
Replicate 2	64.5	39.2

Step 2	$D_{2,1}$ (μm)	$D_{2,2}$ (μm)
Predicted	64.0	51.9
Replicate 1	69.3	55.8
Replicate 2	67.9	58.7

Table 8.2 lists the predicted and experimentally measured values of workpiece distortion after each curing step. The two replicates from the experiment provide a rough idea of the experimental variability. All the predicted values are 5-12% less than the measured values. This consistent difference could the effects of rotational distortion on the workpiece and nonuniform stiffness across the bonding surface. The model established in chapter 6 is based on a workpiece which is held by symmetric supports and will not experience any significant rotational distortion at the bonding location.

This approach provides a reasonable estimate of the polymerization induced distortion in the workpiece of an arbitrary PAAW system. Using this method, a process engineer may evaluate joint curing sequence options and gain insight into how to design a PAAW fixture to minimize distortion at critical features.

Chapter 9

EFFECT OF ADHESIVE BASE RESIN AND FILLER CONTENT ON DISTORTION

This chapter explores the influence of adhesive base resin and filler content on mechanical properties, polymerization shrinkage, and workpiece distortion of several adhesives. This is done through the use of axial load tests, tensile tests, distortion tests, and near-zero stiffness distortion tests.

9.1 Outline of Adhesive Investigation Experiments

9.1.1 Axial Load Tests

Axial Load Tests are designed to assess the effective strength of a PAAW joint. Axial load strength will be a function of adhesive strength at the anvil-adhesive and gripper-adhesive interfaces, the cohesive strength, the degree of polymerization in the secondary cure zone, and any residual stresses in the joint.

For the axial load tests, a 250 style gripper with a 11.7 mm diameter chassis is bonded to a 38 mm diameter aluminum anvil with a turned surface (figure 9.1 shows the hardware used in this experiment). Joint thickness is approximately .89 mm. The adhesive joints were cured for 30 seconds with an Omnicure 2000 lamp with a light intensity of 4 $\frac{W}{cm^2}$ in the 250 to 600 nm range. A tensile testing machine stretches the joint in pure tension at a rate of 12 mm/min. The peak strength measured by the load cell is recorded. Three

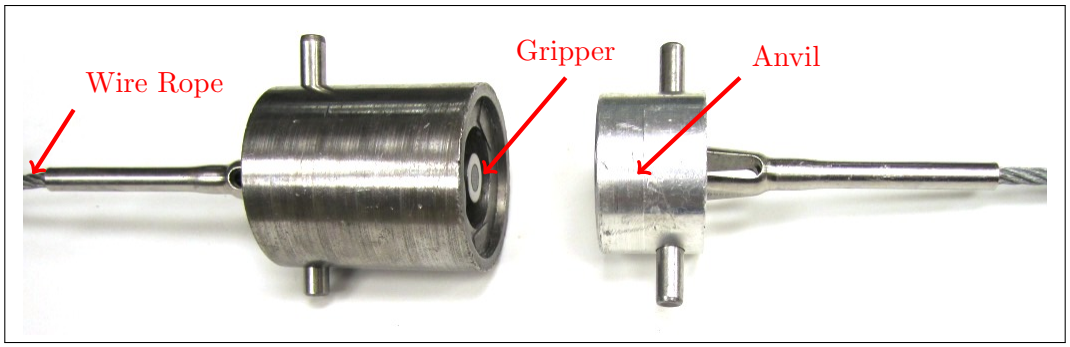

Figure 9.1: Axial load test equipment

replicates were performed for each adhesive.

9.1.2 Workpiece Distortion

The distortion experiments involved bonding a 250 gripper to matching 12.5 mm anvils using the workpiece distortion apparatus. The .64 and 56 $N/\mu m$ beams were chosen to provide a good range in workpiece stiffness. Joint thicknesses of .5 and 1.5 mm were explored. The smaller joints will have an aspect ratio large enough to discourage radial flow which might be possible for the 1.5 mm joint thicknesses.

Like the distortion tests performed earlier in this work, the adhesive is exposed to UV light for 40 seconds. Light provided by a Dymax curing lamp had an intensity of approximately 7-8 W/cm2 in the 250 to 600 nm range.Total anvil displacement is measured at the conclusion of 80 seconds from the beginning of the test. There are two replicates for each combination of levels.

9.1.3 Tensile Properties

Tensile test specimens were created in an aluminum mold coated with a PTFE spray. The specimen follows a modified ASTM D638-10 Type V geometry (figure 9.2). The specimen gage region has nominal cross section dimensions of 3.18 x 3.18 mm and a length of 25.4 mm. Due to the mold creation process, variation in the thickness of the specimens was as great as .25 mm. Each specimen was measured at several locations along the gage region

Figure 9.2: ASTM D638-10 modified type V tensile specimen

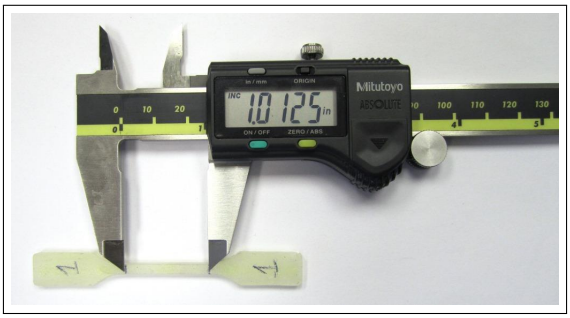

Figure 9.3: Post-fracture measurement of specimen elongation

and the minimum value of thickness was used to compute the values of stress during the test. Care was taken to remove air pockets from the specimen prior to photo-curing. Voids that appear in the back of the specimen were carefully filled with additional adhesive and cured. The specimens were cured with an Omnicure 2000 UV spot lamp for 100 seconds. The test was performed on a United Calibration Tensile Tester using a 250 lbf (1100 N) load cell and a .5-1 (12.7-25.4 mm) extensometer. The machine pulled the jaws apart at a steady 12.7 mm/minute, pausing briefly during the test for the extensometer to be removed, and then continuing on to specimen failure. Specimen elongation post fracture was determined by measuring the distance between the gage region lines of the broken specimen with a digital caliper as illustrated in figure 9.3. Tensile strength and elastic modulus are derived from the stress-strain plot of the test. Three replicates were performed for each adhesive.

9.1.4 Volumetric Shrinkage Approximation

Distortion experiments involving 330 grippers and the .013 $N/\mu m$ beam can be regarded as an implementation of the Bonded Disc Method of Watts and Cash. The beam offers almost negligible resistance, and the 330 grippers provide a large enough diameter to yield

a sufficient aspect ratio for the axial shrinkage to equal the volumetric shrinkage. Near-zero stiffness distortion experiments can be performed using .94 and 1.4 mm nominal joint thicknesses. The 1.4 mm thickness may offer better axial shrinkage measurement resolution and is less influenced by uncertainty regarding the anvil's initial position. However, the .94 thickness offers more resistance to radial flow and has less light transmission losses in the adhesive closest to the anvil. The chassis diameter/thickness ratios for these tests are 15 and 10, respectively. However, considering only the primary cure zone directly above the sapphire, the diameter/thickness ratios are 5.5 and 9.

For their method, Watts and Cash recommend an adhesive drop diameter of at least 9 mm for a 1 mm thickness [11]. However, they used a flexible glass cover slide for the upper bonding substrate, allowing the top surface of the adhesive to behave almost as though it were non-bonded. The steel anvil used in the distortion test apparatus rigidly constrains the top surface of the adhesive, leaving only the perimeter of the adhesive disc non-bonded. Consequently, it may be possible to achieve pure axial shrinkage with much smaller aspect ratios.

9.2 Investigation of Adhesives

This investigation began with an evaluation of a variety of base resins without any significant filler content. Table 9.1 lists general properties of these base resins. The GB series is intended for bonding to glass; the current PAAW adhesives are built off of this resin. The PB "plastic bonding" resins will dissolve polymers to promote strong bonds to plastics. UB is a "universal bonder" formulated for adhering to many types of substrate materials. PSA is a UV curable pressure sensitive adhesive.

A set of preliminary axial load and distortion experiments concluded that the PB0 and DC0 have potential for making low distortion adhesives of acceptable strength. These resins were modified with the following additions:

- Higher concentrations of photo-initiators to increase secondary cure zone polymeriza-

Table 9.1: UV curable base resins

	Class	Viscosity (cP)	Volumetric Shrinkage	Tensile (MPa)
GB0*	Acrylate	205	8.4%	15.8
DC0	Hybrid Acrylate	1000	5.7%	7.1
PB0	Urethane Acrylate	3500	9.0%	3.3
UB0	Urethane Acrylate	3000	5.8%	2.2
PSA0	Acrylic	4500		

$*$ Provided for reference, but not evaluated in this work.
Data courtesy of CTECH LLC
The adhesive naming convention is unique to this document and does not reflect the trade names of these products

tion

- Fumed silica to give the resins a gel consistency for easier application on grippers
- Various types of filler content to reduce shrinkage

The GB series adhesives is already in use in the PAAW application. Since they have already been developed to have a sufficient concentration of fumed silica and photo-initiators, these adhesives were modified by adding only filler content.

The Plastic Bonder series was used to explore the effects of a variety of filler materials. Table 9.2 lists the compositions of these adhesives. The effective joint strengths (9.7) of these adhesives were inadequate for the PAAW application and consequently these did not undergo the full set of characterization experiments. However, these adhesives provide some insight into the behavior of the filler materials in the base resin. PB1 and PB2 suffered from filler separation; the glass balloons were much less dense than the base resin and the viscosity of the adhesive was insufficient to prevent separation. This effect was much more pronounced in PB1 because larger microballoons have a lower density. From figure 9.4, the effect of the filler materials on the adhesive's appearance can be seen. The 35 micron balloons scatter light, making PB1 appear white in color. The 200 nm spheres are smaller than the wavelength of visible light, so they have little effect on the adhesive's optical

Table 9.2: PB series filled adhesives

	Filler Type	Filler %wt	Fumed Silica %wt
PB1	35 μm SiO_2 balloons	11.5%	4.6%
PB2	200 nm SiO_2 balloons	34%	
PB3	120 μm SiO_2 spheres	34%	3.7%
PB4			4.5%

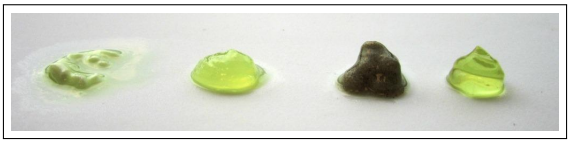

Figure 9.4: Adhesives: PB1, PB2, PB3, PB4

properties; it closely resembles PB4. The large glass spheres give PB3 the texture and appearance of sand.

The composition of the modified DC series adhesives can be found in table 9.3. Several of these adhesives have promising mechanical properties, and are investigated thoroughly. DC0F was created in Penn State University by adding ground polymerized GB1 as filler to DC0. These adhesives bond readily to plastic, especially plastics with similar composition. Compared to glass fillers, plastic filler will not substantially increase the effective elastic modulus and may better halt the development of cracks. However, the quantity of this adhesive was insufficient for performing all of the characterization experiments. Figure 9.5 shows the DC series adhesives. As seen in the PB series, the addition of glass balloons to the base resin gives DC2 its opaque white appearance. However, unlike PB1 and PB2, the

Table 9.3: DC series filled adhesives

	Filler Type	Filler %wt	Fumed Silica %wt
DC1			5.8%
DC2	200 nm SiO_2 balloons	26%	1.1%
DC0F	Ground GB1	19%	

Figure 9.5: DC series adhesives: DC0, DC1, DC2

Table 9.4: GB series adhesives

	Filler Type	Filler %wt	Fumed Silica %wt	Impact Modifier %wt	Notes
GB1			2.9%	9.8%	Adhesion promoters
GB2			2.9%	9.8%	No adhesion promoters
GB3	60 μm SiO_2 spheres	66%	1.0%	3.3%	Filler added to GB2
GB1F	Ground GB1	25%	2.2%	7.3%	Filler added to GB1

DC resin is not prone to filler separation.

Table 9.4 lists the properties of adhesives built on the Glass Bonder product base. GB2 and GB1 were formulated prior to this investigation and form the backbone of PAAW. This series of adhesives contains rubber impact modifiers to give the joints the toughness necessary to survive loading conditions in heavy milling operations. GB2 was designed for bonding to ceramic workpieces and lacks adhesion promoters to minimize damage to the workpiece during debonding. It is thought that the lack of adhesion will allow greater radial flow of the adhesive during polymerization and consequently reduce the workpiece distortion. GB1F was the second filled adhesive created in-house by adding ground GB1 particles to uncured GB1 adhesive. The appearance of these adhesives prior to photo-curing can be seen in 9.6.

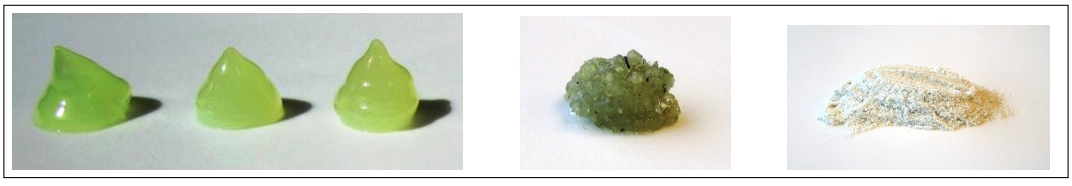

Figure 9.6: GB series adhesives: GB1, GB2, GB3, GB1F, and ground GB1 powder

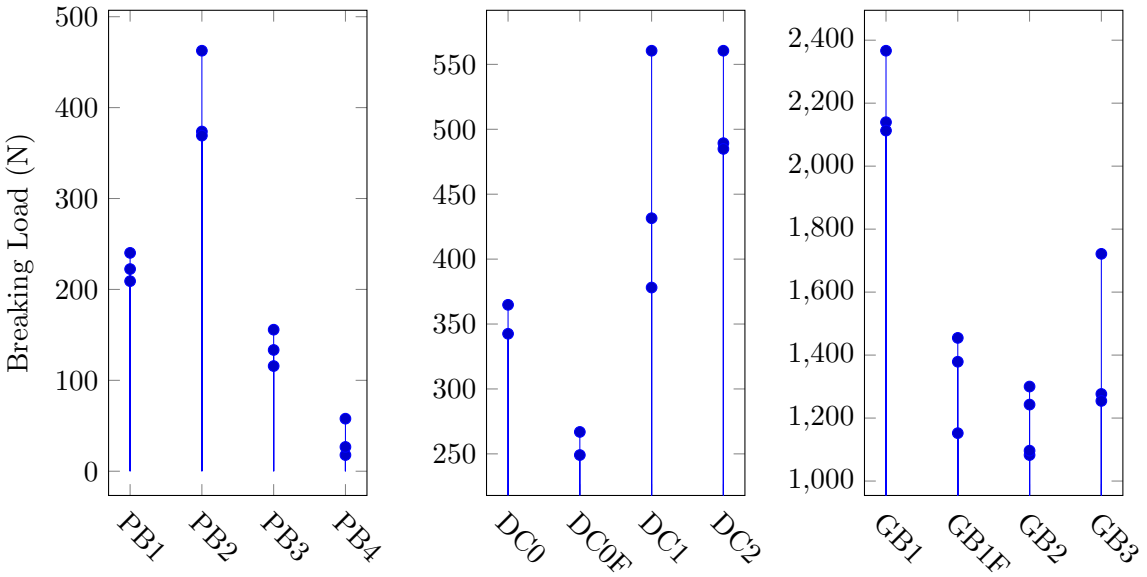

Figure 9.7: Axial load tests of PB, DC, and GB series adhesives with .89 mm joint thickness and 30 second exposure to 4 W/cm^2 of 250 nm 600 nm light

9.3 Results of Adhesive Investigation

Figure 9.7 shows the results of the axial load tests on the PB, DC, and GB series adhesives. The PB series were far to weak to merit any further investigation. The polymerized filler content decreased the axial load strength of the DC0 and GB1 adhesives. The ground plastic may have greatly reduced the transmission of UV light through the adhesive and resulted in a significant reduction of degree of conversion. The coarse surface texture of the ground particles may trap air and increase the light scattering at the particle-adhesive interface. On the other hand, the glass based fillers appeared to increase the axial load strength.

Figure 9.8 shows a comparison of distortion resulting from the GB and DC adhesives at typical levels of workpiece compliance and joint thickness. Two replicates were performed for most combinations.

The effects of using ground polymer filler can be seen in figure 9.9. The polymer filled

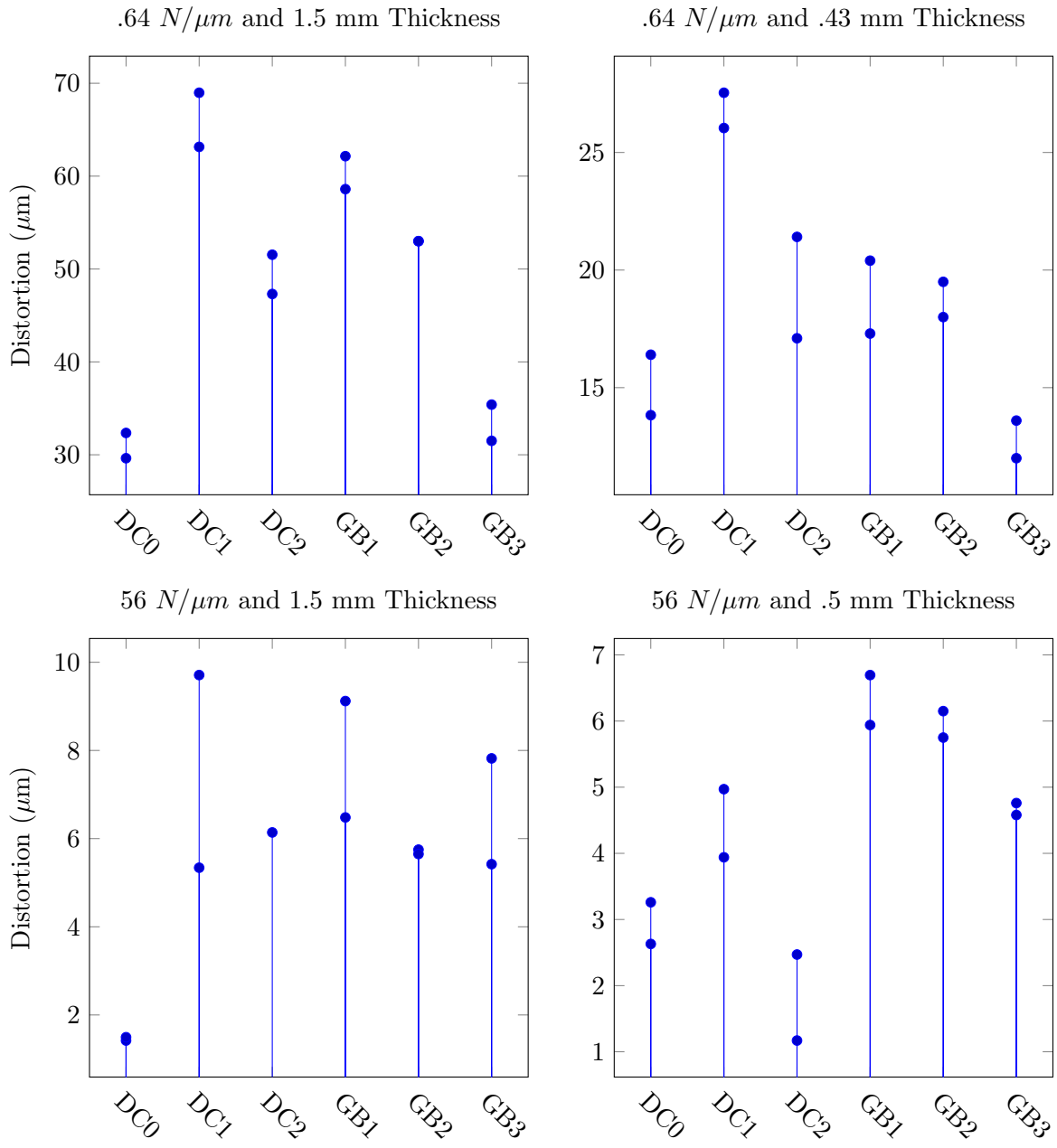

Figure 9.8: Worpiece distortion from adhesives with varying workpiece stiffness and joint thickness

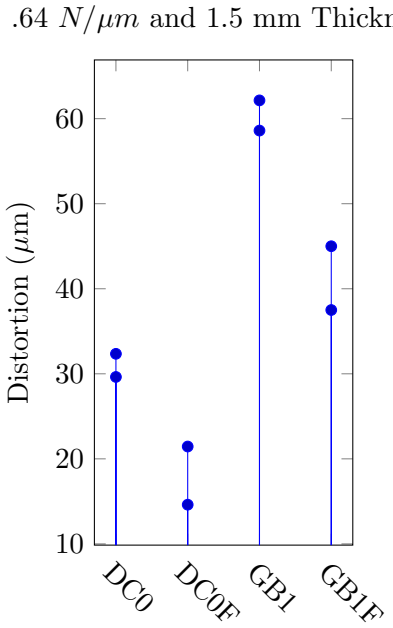

Figure 9.9: Effect of ground polymer filler on workpiece distortion. .64 $N/\mu m$ workpiece stiffness and 1.5 mm joint thickness

adhesives show a clear reduction in distortion.

Figure 9.10 shows a typical tensile test of an adhesive specimen. An extensometer was used to obtain strain data in the elastic region for deriving the elastic modulus but it must be removed before the material approaches its yield point. If it is removed too late, the specimen will begin plastically deforming prematurely at the knife edge of the extensometer and may suddenly fail at that point. The crosshead position of the machine for the full duration of the test is shown in the figure to provide insight into the behavior of the specimen. However, note that crosshead position data does not accurately reflect the gage region displacement of the specimen. The slight discontinuity in the plot corresponds to when the machine halted for 1-2 seconds for the extensometer to be removed.

The moment that the machine halts, the specimen will rapidly begin relaxing its stress. Figure 9.11 shows the effect of holding the specimen at a constant displacement for some time.

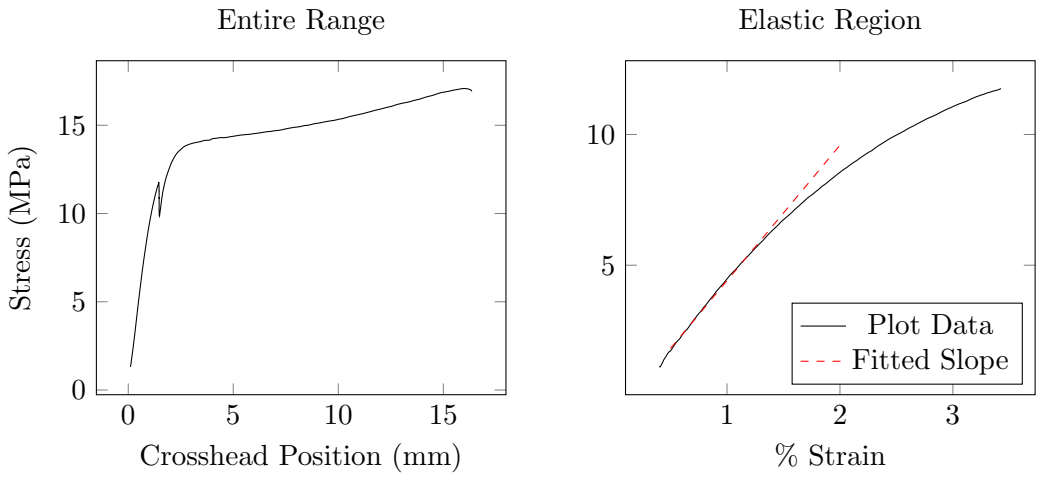

Figure 9.10: ASTM D638-10 tensile test of GB1 with extension rate of 12.7 mm/min

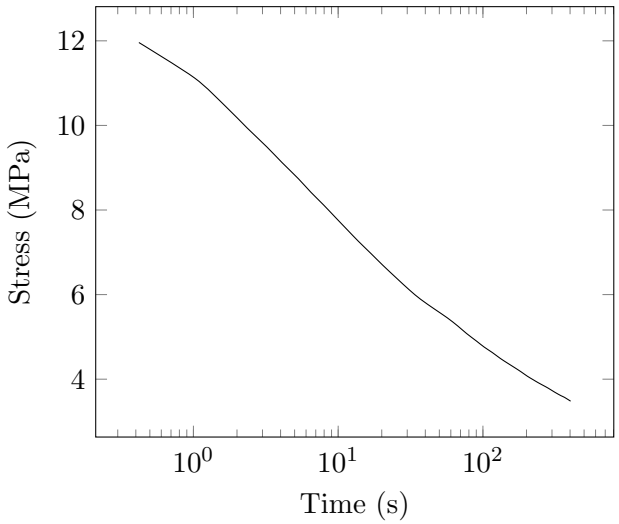

Figure 9.11: Stress relaxation of GB1 tensile specimen held under constant displacement

Tensile tests were performed on the GB1, GB2, GB3, DC0, DC1, and DC2 adhesives. The tensile strength, elastic modulus, and ductility can be found in figure 9.12. The large variation in elastic modulus and tensile strength could be due to inhomogeneity of the adhesive samples and the presence of voids caused by trapped air. All of the adhesives are prone to trapping air; however voids are particularly problematic for the glass-filled variants

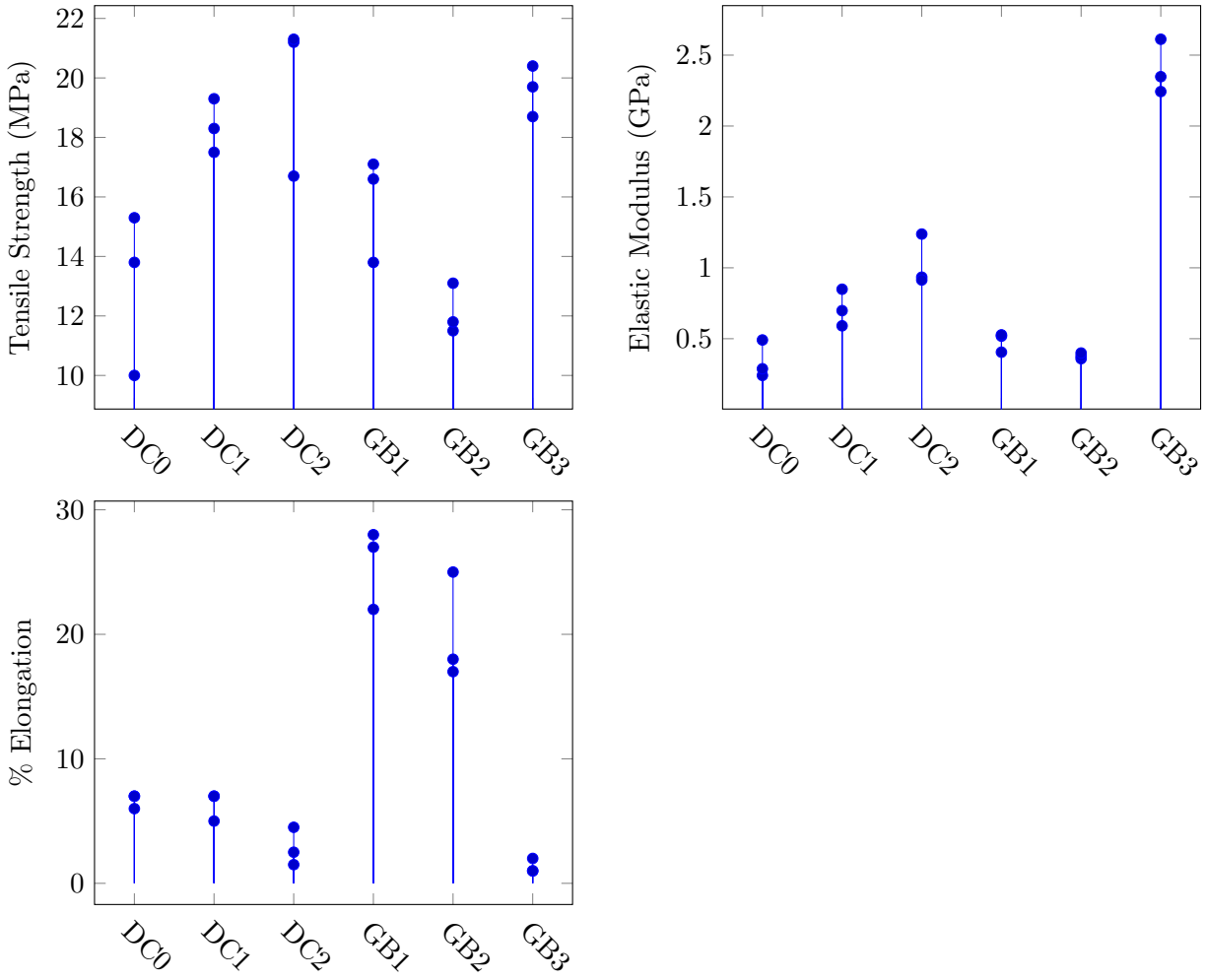

Figure 9.12: Properties derived from ASTM D638-10 tensile test with 12.7 mm/min strain rate, showing 3 replicates per sample

due to their greater viscosity.

Figure 9.13 shows a comparison of the approximate volumetric shrinkage of GB1, GB2, DC1, and their filled variants determined using the distortion test apparatus with 330 grippers and the .013 $N/\mu m$ beam.

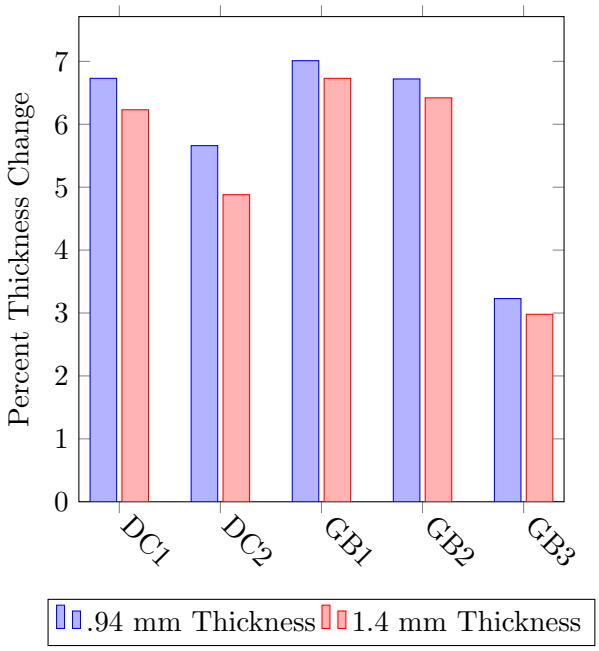

Figure 9.13: Axial shrinkage estimation with 330 grippers and .013 $N/\mu m$ workpiece stiffness

9.4 Discussion of Adhesive Investigation

9.4.1 Bonding Strength Estimation

The adhesive tensile strength of an adhesive that fails by debonding from the gripper or anvil in an axial load test can be estimated by dividing the peak force by the surface area of the gripper. This will not take into account local variations in adhesive strength due to differences in degree of conversion across the joint or the effect of stress concentrations. However, it may provide a rough idea of the relative difference in the adhesive and cohesive strength. Using this method, the adhesive tensile bonding strengths of DC1 and DC2 are approximately 3.5-5.2 MPa and 4.5-5.2 MPa, respectively. These values are about 20-30% the cohesive tensile strengths determined through tensile testing.

Applying this approach to an adhesive joint that fails in a cohesive manner can be used to approximate the cohesive tensile strength. For GB1 and GB2, the approximate cohesive tensile strengths are 16.1-18.4 MPa and 10.1-12.1 MPa, respectively. These values line up

surprisingly well with the tensile test results.

The failure mode of a joint in an axial load test has important practical consequences. Joints with an adhesive strength much smaller than its cohesive strength would not be appropriate for a heavy machining operation since the joints may fail unpredictably. However, these adhesives present a distinct advantage for non-contact manufacturing operations and part inspection: The ease at which the adhesive debonds greatly simplifies the removal of polymerized joint remnants after workpiece debonding.

9.4.2 Volumetric Shrinkage Estimation

The method using the distortion apparatus with 330 grippers and .013 $N/\mu m$ beam can provide a reasonable estimate of the total volumetric polymerization shrinkage of an adhesive. However, it does involve a fair amount of error. For instance, the consistent difference in estimated volumetric shrinkage for the two joint thicknesses could be the result of one of several possible effects:

- Measurement uncertainty of the initial joint thickness
- Radial flow of adhesive during polymerization
- Differences in average degree of conversion resulting from changes in light transmission and scattering.

Most likely, it is due to measurement uncertainty of the thickness. Unlike the other beams, the .013 $N/\mu m$ beam deflects approximately .03 mm under the weight of the anvil. To make matters worse, the uncured adhesive often has enough viscosity to partially support the anvil, making the precise anvil position prior to curing difficult to determine.

The results of this method agree with the expected decreases in shrinkage from the addition of inert filler. The estimated volumetric shrinkage of the GB3 was approximately 46-48% of its unfilled counterpart, GB2. This is expected since GB3 has 45% nominal volume fraction of inert filler. This volume fraction was calculated from the weight percentage

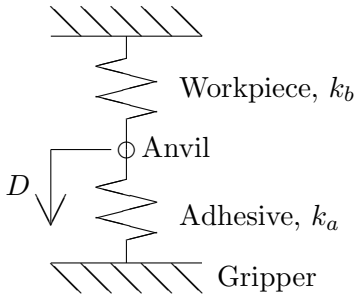

Figure 9.14: Simple spring model

of filler and the densities of the GB adhesive base resin and SiO_2. Due to uncertainty regarding the average diameter and wall thickness of the microballons in DC2, its filler volume fraction was not computed.

The difference in estimated volumetric shrinkage of GB1 and GB2 may be a consequence of some of the factors described above. There is little reason to believe that the addition of adhesion promoters would cause a significant increase in volumetric shrinkage. Rather, the lack of adhesion promoters of GB2 may have allowed the adhesive to experience some flow in the radial direction that detracted from axial shrinkage.

9.4.3 Correlation Between Tensile Properties, Volumetric Shrinkage, and Distortion

The best way to understand the effects that the properties of the adhesives have on workpiece distortion is to build a first principles model that accounts for the more readily apparent phenomenon, such as volumetric shrinkage and elastic strain. A simple model of the workpiece and adhesive joint can be constructed using two linear springs in series (figure 9.14). The point joining both springs represents the position of the anvil.

Polymerization shrinkage will decrease the length of the adhesive spring. This decrease in length is equal to $\beta \cdot t \cdot r$ where β is the volumetric shrinkage factor, t is the original joint

thickness, and r is a coefficient that accounts for the relative amount of radial adhesive motion during polymerization. r is a function of many factors including joint thickness, workpiece stiffness, adhesive viscosity, adhesive strength, and rate of polymerization.

The new position of the anvil, or the distortion as measured by the test apparatus, is given by the following equation:

$$D = \frac{k_a}{k_a + k_b} \cdot \beta \cdot t \cdot r \tag{9.1}$$

Here, k_a is the effective joint stiffness and k_b is the effective beam or workpiece stiffness. If it is assumed that the joint's average elastic modulus is equal to the value determined through tensile testing, then $k_a = \frac{E \cdot A}{t}$. E is the elastic modulus and A, the joint cross sectional area, is approximately the gripper surface area, or 122 mm^2 for a 250 gripper. For compliant workpieces, such as the .64 $N/\mu m$ beam, $\frac{k_a}{k_a + k_b}$ is very close to unity.

Figure 9.15 shows the computed r coefficient as a function of both workpiece stiffness and joint thickness. The coefficient r was computed from the following equation:

$$r = \frac{D}{\frac{k_a}{k_a + k_b} \cdot \beta \cdot t} \tag{9.2}$$

with $k_a = \frac{E \cdot A}{t}$

The values of E, β, and D were taken as the average of the experimental results for each adhesive. DC0 was not included because it fails to fully polymerize the secondary cure region. The differences in r coefficient between adhesives at several of the levels indicates that some of the other factors mentioned above may be significant. However, there is no correlation between r coefficient and elastic modulus or cohesive strength. Interestingly, the DC series adhesives exhibit a relatively low r value at the 56 $N/\mu m$ & .5 mm level. The reason for this is unclear; it may simply be the result of experimental error.

The addition of 60 micron glass spheres increases the r coefficient in the GB series adhesive; however, filler content decreases r in the DC series. This may have to do with

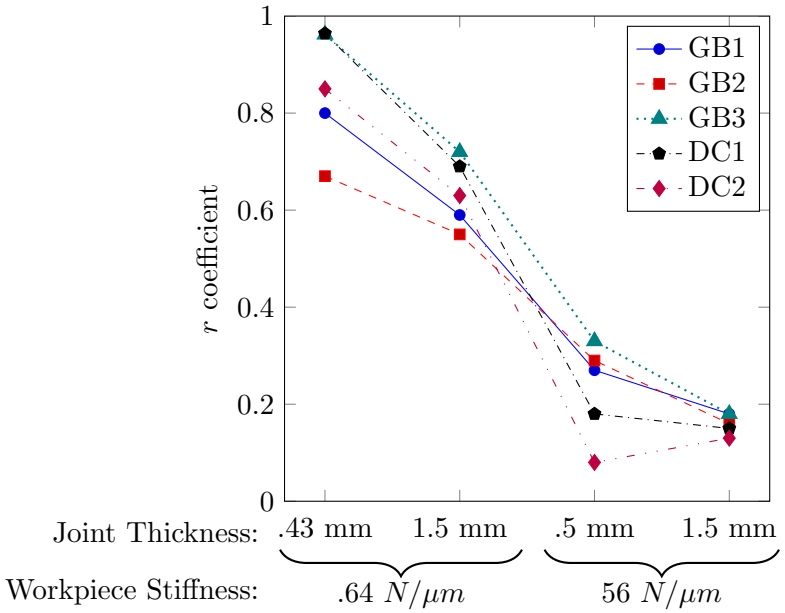

Figure 9.15: r coefficient as a function of workpiece stiffness and joint thickness for various adhesives

the effect of filler on light transmission. The hollow spheres in DC2 scatter light and give the adhesive a white appearance. This may slow the polymerization kinetics, allowing more time for stress relaxation, or reduce degree of conversion in the secondary cure zone. Either of these will reduce workpiece distortion.

Although DC0 was not included in this comparative study, it is worth discussing a very counterintuitive behavior it exhibits. DC0 caused substantially less distortion in the 56 $N/\mu m$ workpiece when the joint thickness is smaller (see figure 9.8). In terms of the model presented above, the r coefficient of DC0 must be small for the 56 $N/\mu m$ stiffness and 1.5 mm thickness combination and many times larger with .5 mm thickness for the same level of stiffness. One possible physical explanation for this is as follows: DC0 lacks the amount of photo-initiators needed to fully cure the secondary cure zone. As a result, the aspect ratio of the polymerizing region of the 1.5 mm joint may be considerably smaller than that of typical joints. This combined with DC0's slow rate of polymerization and low viscosity

may allow for comparatively large amounts of radial flow for the 1.5 mm joint. The .5 mm joint, on the other hand, may have an aspect ratio sufficient to resist radial flow.

Another interesting observation involves the distortion caused by DC0F (also not included in the comparative study). DC0F had a viscosity comparable to DC1 and exhibited much less distortion. This adhesive was rather opaque and, lacking numerous photoinitiators, may have suffered from a reduced degree of conversion. This is supported by its much lower axial load strength than the other DC series adhesives.

Chapter 10

SUMMARY AND FUTURE WORK

10.1 Summary

Chapter 5 described the design, principal features, and operation of an apparatus for experimentally measuring the workpiece distortion resulting from photo-curing adhesive joints with varying amounts of workpiece stiffness and joint thickness.

This apparatus was first used in chapter 6 to characterize the response of adhesive GB1 to a range of workpiece stiffnesses and joint thicknesses. Empirical models were developed and fitted to the experimental data to describe the distortion as a function of the these two variables and as a function of residual force in the joint.

Chapter 7 explored the differences in polymerization rate in the primary and secondary cure zones. An experiment where the diameter of the adhesive joint was varied showed that for a low workpiece stiffness, the primary cure zone appears to resist any further distortion that would otherwise be caused by the secondary cure zone. However, this does not appear to be the case for stiffer workpieces where the stiffness of the polymerized primary zone does not have as great a contribution to the overall system stiffness. In this chapter, the soft start light exposure cycle was briefly investigated. By initially exposing the joint to 1 second of light and then closing the lamp shutters for a length of time before fully curing the joint, the distortion was reduced by 25%. It is believed to be a result of partially polymerizing the primary zone well before the secondary zone and a slower reaction rate.

In chapter 8, the resulting distortion from curing multiple joints either sequentially or simultaneous to a workpiece was experimentally measured and compared to the distortion of curing each joint individually. In addition, this chapter presented a methodology for predicting the distortion of a workpiece for sequential curing sequences. For each step in the sequence, the stiffness matrix of the system can be determined through finite element analysis. Using the single joint model fitted in chapter 6, the distortion vector of the workpiece from that joint can be computed. The linear sum of the distortion at each step yields the predicted total distortion of the curing sequence. A case study shows how this method can produce estimates that are reasonably close to experimentally derived results.

The mechanical properties and workpiece distortion characteristics of a variety of adhesives were determined in chapter 9 through tensile tests, axial load tests, and distortion tests. Glass filler content increased the elastic modulus, and in some cases, tensile strength, but drastically reduced the ductility. By using a .013 N/μm workpiece stiffness, the volumetric shrinkage of the adhesives was measured. As expected, the filler content decreased volumetric shrinkage by the volume fraction of the filler. For the distortion tests, a model was created to account the effects of the volumetric shrinkage percentage and elastic strain of the adhesives. This left a coefficient, named here as r, to represent the tendency of the adhesives to draw radially inward rather than shrink axially for a particular workpiece stiffness and joint thickness combination. This r coefficient serves as an additional basis for comparing the workpiece distortion characteristics of adhesives.

10.2 Discussion

As a whole, this thesis presented an investigation of the factors that contribute to workpiece distortion in an adhesive workholding system. From a macroscopic point of view, this work looked into and empirically modeled the net distortion induced by PAAW joints on workpieces. Then, it offered an explanation of how a non-uniform curing light distribution in an adhesive joint may account for the behavior of a curing PAAW joint and the result-

ing distortion. Next, these concepts and models were used as building blocks to create a methodology for understanding workpiece distortion in any arbitrary PAAW fixture. In addition, this work explored several ideas in the literature on how to minimize workpiece distortion, such as through soft start curing and adding inert filler content to adhesives. The strategy of modifying the adhesive to promote minimal distortion was investigated in depth and the influence of the adhesive's mechanical properties on distortion were examined. In short, this thesis has presented an outline of concepts and experimental results that can guide a process engineer in designing an adhesive fixturing system for minimizing workpiece distortion.

10.3 Future Work

There are a number of areas for further investigation to shed more light on the behavior of the adhesives during polymerization and the resulting workpiece distortion.

The intensity and spectrum of the curing light is an important variable that will affect the distortion behavior of the adhesive joints. Lower light intensity generally results in a reduced polymerization rate and less workpiece distortion. It is believed that greater light intensity will widen the primary cure zone and increase distortion by increasing the primary zone aspect ratio. A model that captures the effect of light intensity and spectrum may provide some additional insight into how the adhesive behaves as it cures and assist the end user in determining the optimal intensity for minimizing distortion and cycle time.

As discussed in section 7.4, a soft start curing scheme can reduce the distortion by a considerable amount. More work is needed to determine whether this reduction is affected by the other variables, such as joint thickness, workpiece stiffness, and adhesive composition. In addition, the mechanical properties of a soft-start cured joint are unknown. It is possible that by allowing the primary cure zone to polymerize much earlier than the secondary zone, a reduced optical transmittance of the polymerized primary zone may block light from entering the secondary zone and reduce its degree of conversion and consequently its

strength. To verify this idea, it would be necessary to perform axial load tests on soft-start cured joints.

This is related to the broader topic of optimal curing cycle for low distortion, adequate strength, and reasonable cycle time. The initial exposure duration and intensity is worthy of further investigation. Another set of parameters to determine are the start time, duration, and intensity of the second exposure. It may not necessarily be the case that one must wait for the distortion to reach steady state before initiating subsequent exposures. One strategy may be to pulse the light at a certain frequency and pulse duration to keep the polymerization reaction proceeding at a reasonable rate while reducing the overall heat input from the curing light. This may minimize the distortion due to thermal contraction as the joint cools.

From the thermal contraction curve in the distortion plots (figure 5.16), it is evident that the adhesive reaches an elevated temperature during the cure. Depending on the peak temperature, the adhesive may thermally soften and allow for some stress relaxation by means of viscous flow. The extent of this stress relaxation, if it does occur, could be determined with carefully designed distortion experiments. Peak temperature and the temperature profile in the joint may be measured with an infrared radiometer or thermocouples. These temperatures can also be predicted using knowledge of the adhesive's thermal and optical properties, the enthalpy of the polymerization reaction, the curing light power input, and the thermal properties of the workpiece and gripper. This combined with the storage and loss moduli determined through dynamic mechanical analysis can be used to construct a model to estimate how much thermal stress relaxation affects to the distortion caused by a PAAW joint.

In section 9.4.2, it was assumed that by using a 330 style PAAW gripper and a .013 N/μm beam in the distortion test apparatus, the volumetric shrinkage factor could be determined. Although this approach bears great resemblance to the Bonded Disc Method discussed in the literature, there remains slight uncertainty as to whether the aspect ratio

of the primary cure zone of a joint on a 330 gripper is sufficient for pure axial shrinkage. The volumetric shrinkage of the adhesives used in this work should be evaluated using alternative methods, such as optically or with a water or mercury dilatometer. Comparison of these shrinkage values will show conclusively whether the distortion test apparatus can be used to accurately determine volumetric shrinkage of adhesives.

This work looked only at a few sizes of both solid and hollow glass filler content. Evaluating other types of filler particles and finding the optimal filler size could be the subject of further investigation. Other filler ideas include the following:

- Particles which by virtue of their chemistry or applied coatings, form very weak bonds with the adhesive
- Very low elastic modulus materials, such as polymers
- Fiber or platelet shaped particles
- Ferromagnetic fibers that can be aligned along the axis of an adhesive joint with an applied magnetic field

Chapter 8 provides a thorough examination of how to predict workpiece distortion for a sequential cure. However, it does not address methods of modeling simultaneous cures where all joints are exposed to light at the same time. Figure 8.1 shows that, compared to joints curing individually, the relative distortion of a simultaneous cure is a function of joint thickness and possibly the workpiece stiffness matrix. A model for predicting this behavior may involve minimizing the total strain energy of the system while taking into account how the changing system stiffness affects radial flow of the adhesive. Whether an analytical closed form solution can be derived for an arbitrary system or if the system must be numerically simulated is to be determined.

Of practical interest for predicting sequential and simultaneous cures is how to deal with uncertainty regarding joint thickness. One of the key advantages of a PAAW fixture is its ability to tolerate variation in joint thickness from .2 to 3 mm. Knowing the range of

variation of the bonding sites on the workpiece, it would be useful to have an efficient way of predicting the range of workpiece distortion for each critical feature.

References

[1] De Meter, E. C. Light activated adhesive gripper (laag) workholding technology and process. *Journal of Manufacturing Processes*, 6(2):201–214, 2004.

[2] Kaur, M. and Srivastava, A. K. Photopolymerization: A review. *Journal of Macromoecular Science, Part C - Polymer Reviews*, C42(4):481–512, 2002.

[3] Slopek, R. P. In-situ monitoring of the mechancial propertiesduring the photopolymerization of acrylate resins using particle tracking microrheology. 2008.

[4] Endruweit, A. Johnson, M. S., and Long, A. C. Curing of composite components by ultraviolet radiation: A review. *Polymer Composites*, 27:119–128, 2006.

[5] Baker, C. C., and De Meter, E. C. Investigation of a critical irradiance criterion for minimizing the cure time of a paw joint. *Journal of Adhesion Science and Technology*, 24:1303–1317, 2010.

[6] De Meter, E. C., and Kumar, J. S. Assessment of photo-activated adhesive workholding (paw) technology for holding "hard-to-hold" workpieces for machining. *Journal of Manufacturing Systems*, 29:19–28, 2010.

[7] Raffles, M. H., Kollur, K., Axinte, D., and Llewellyn-Powell, H. Assessment of adhesive fixture system under static and dynamic loading condtions. *Proceedings of the Institution of Mechanical Engineers Part B: Journal of Engineering Manufacture*, 227(2):267–280, 2013.

[8] Haq, J., Vogt, B., Howard, E., and Loy, D. Temporary bond-debond technology for high-performance transistors on flexible substrates. *Journal of the SID*, 18(11):884–891, 2010.

[9] Cai, W., Hu, S. J., Yuan, J. X. Deformable sheet metal fixturing: Principles, algorithms, and simulations. *Journal of Manufacturing Science and Engineering*, 118:318–324, 1996.

[10] Watts, D.C., and Cash, A.J. Determination of polymerization shrinkage kinetics in visible-light-cured materials: Methods development. *Dental Materials*, 7:281–287, 1991.

[11] Watts, D.C., and Marouf, A.S. Optimal specimen geometry in bonded-disk shrinkage measurements on light-cured biomaterials. *Dental Materials*, 16:447–451, 2000.

[12] Lee, I., Cho, B., Son, H., Um, C., and Lim, B. The effect of consistency, specimen geometry and adhesion on the axial polymerization shrinkage measurement of light cured composites. *Dental Materials*, 22:1071–1079, 2006.

[13] Hudson, A., Martin, S., Hubert, M., and Spelt, J. Optical measurements of shrinkage in uv-cured adhesives. *Journal of Electronics Packaging*, 124:352–354, 2002.

[14] Dauvillier, B. S., Hubsch, P. F., Aarnts, M. P., Feilzer, A. J. Modeling of viscoelastic behavior of dental chemically activated resin composites during curing. *Journal of Biomedical Material Research (Applied Biomaterials)*, 58:16–26, 2001.

[15] Min, S., Ferracane, J., and Lee, I. Effect of shrinkage strain, modulus, and instrument compliance on polymerization shrinkage stress of light-cured composites during the initial curing stage. *Dental Materials*, 26:1024–1033, 2010.

[16] Braem, M., Lambrechts, P., Van Doren, V., Vanherle, G. The impact of composite structure on its elastic response. *Journal of Dental Research*, 65(5):648–653, 1986.

[17] Labella, R., Lambrechts, P., Van Meerbeek, B., and Vanherle, G. Polymerization shrinkage and elasticity of flowable composites and filled adhesives. *Dental Materials*, 15:128–137, 1999.

[18] Kleverlaan, C. and Feilzer, A. Polymerization shrinkage and contractoin stress of dental resin composites. *Dental Materials*, 21:1150–1157, 2005.

[19] Lee, S. H., Chang, J., Ferracane, J., Lee, I. B. Influence of instrument compliance and specimen thickness on the polymerization shrinkage stress measurement of light-cured composites. *Dental Materials*, 23:1093–1100, 2007.

[20] Laughlin, G., Williams, J., and Eick, J. The influence of system compliance and sample geometry on composite polymerization shrinkage stress. *Journal of Biomedical Material Research (Applied Biomaterials)*, 63:671–678, 2002.

[21] Petrovic, L. and Atanackovic, T. A model for shrinakge strain in photo polymerization of dental composites. *Dental Materials*, 24:556–560, 2008.

[22] Patankar, K., Dillard, D., and Fernholz, K. Characterizing the constitutive properties and developing a stress model for adhesive bond-line readout. *International Journal of Adhesion and Adhesives*, 40:149–157, 2013.

[23] Castagnetti, D., and Dragoni, E.. Standard finite element techniques for efficient stress analysis of adhesive joints. *International Journal of Adhesion and Adhesives*, 29:125–135, 2009.

[24] De Meter, E. C. Characterization of the quasi-static deformation of laag joints adhering machined steel surfaces. *Journal of Manufacturing Science and Engineering*, 127(2):350–357, 2005.

[25] Lee, J. D., and Haynes, L. S. Finite-element analysis of flexible fixturing system. *Journal of Manufacturing Science and Engineering*, 109:134–139, 1987.

[26] Baker, C. C., and De Meter, E. C. Modeling and analysis of the irradiance of incipient curing light reaching the adhesive-workpiece interface within a laag joint. *Journal of Adhesion Science and Technology*, 22:1105–1121, 2008.

[27] Satterthwaite, J.D., Vogel, K., Watts, D.C. Effect of resin-composite filler particle size and shape on shrinkage-strain. *Dental Materials*, 25:1612–1615, 2009.

[28] Miao, X., Li, Y., Zhang, Q., Zhu, M., and Wang, H. Low shrinkage light curable dental nanocomposites using SiO_2 microspheres as fillers. *Materials Science and Engineering C*, 32:2115–2121, 2012.

[29] Garoushi, S., Vallittu, P., Watts, D., and Lassila, L. Effect of nanofiller fractions and temperature on polymerization shrinkage on glass fiber reinforced filling material. *Dental Materials*, 24:606–610, 2008.

[30] Braga, R.R., Ballester, R.Y., and Ferracane, J.L. Factors involved in the development of polymerization shrinkage stress in resin-composites: A systematic review. *Dental Materials*, 21:962–970, 2005.

[31] Lim, B., Ferracane, J., Sakaguchi, R., and Condon, J. Reduction of polymerization contractoin stress for dental composites by two-step light-activation. *Dental Materials*, 18:436–444, 2002.

[32] Versluis, A., Douglas, W.H., Cross, M., and Sakaguchi, R.L. Does an incremental filling technique reduce polymerization shrinkage stresses? *Journal of Dental Research*, 75(3):871–878, 1996.